LBL-24218
Preprint

Lawrence Berkeley Laboratory
UNIVERSITY OF CALIFORNIA

Materials & Chemical Sciences Division

RECEIVED
LAWRENCE
BERKELEY LABORATORY

JAN 3 1988

LIBRARY AND
DOCUMENTS SECTION

Submitted to Acta Metallurgica

Effect of Quench Rate on the Intrinsic Coercivity of Iron/Rare Earth/Boron Permanent Magnets

R. Ramesh and G. Thomas

November 1987

TWO-WEEK LOAN COPY
This is a Library Circulating Copy
which may be borrowed for two weeks.

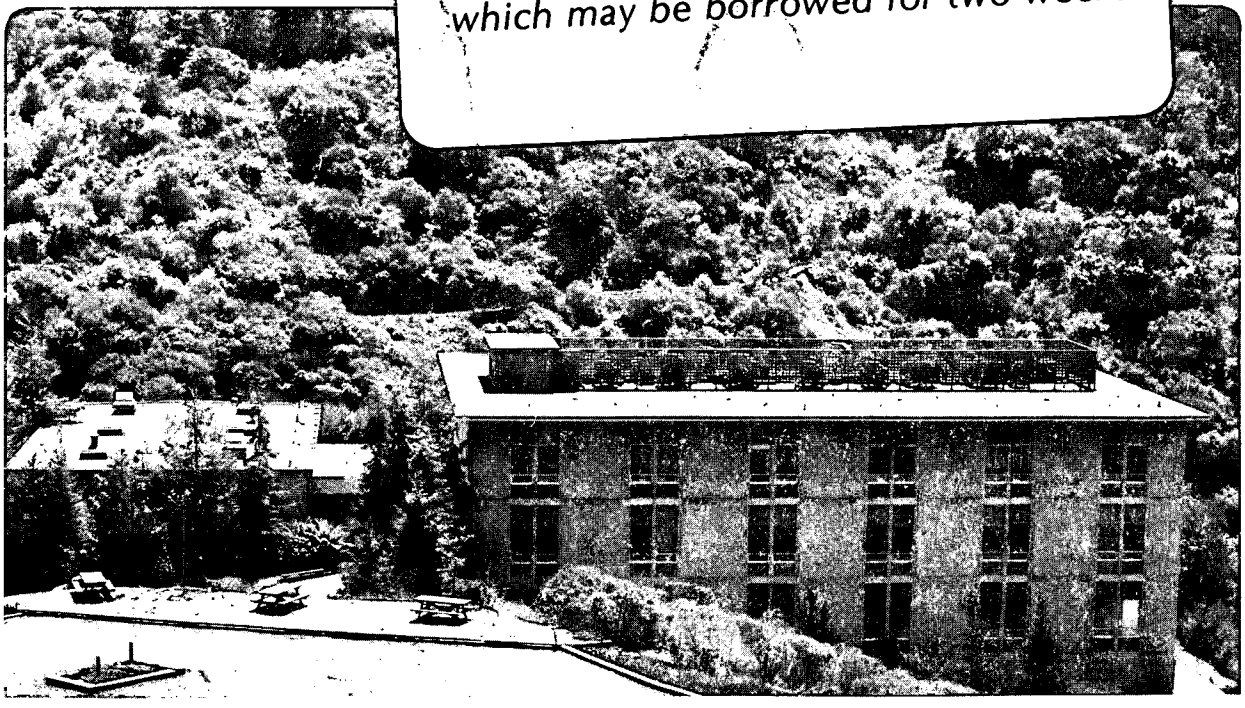

LBL-24218 c.2

Prepared for the U.S. Department of Energy under Contract DE-AC03-76SF00098

DISCLAIMER

This document was prepared as an account of work sponsored by the United States Government. While this document is believed to contain correct information, neither the United States Government nor any agency thereof, nor the Regents of the University of California, nor any of their employees, makes any warranty, express or implied, or assumes any legal responsibility for the accuracy, completeness, or usefulness of any information, apparatus, product, or process disclosed, or represents that its use would not infringe privately owned rights. Reference herein to any specific commercial product, process, or service by its trade name, trademark, manufacturer, or otherwise, does not necessarily constitute or imply its endorsement, recommendation, or favoring by the United States Government or any agency thereof, or the Regents of the University of California. The views and opinions of authors expressed herein do not necessarily state or reflect those of the United States Government or any agency thereof or the Regents of the University of California.

MICROSTRUCTURE AND PROPERTIES OF RARE EARTH MAGNETS

R.RAMESH[1], J.K.CHEN[1], L.K.RABENBERG[2] and G.THOMAS[1,#]

1 Department of Materials Science and Mineral Engineering and Materials and Chemical Sciences Division, Lawrence Berkeley Laboratory, University of California, Berkeley, Ca94720.

Scientific Director, National Center for Electron Microscopy, LBL, University of California, Berkeley, Ca94720.

2 Center for Materials Science and Engineering, The University of Texas at Austin, Austin, Texas 78712.

A. GENERAL INTRODUCTION

Permanent magnets represent the oldest "electronic" material ever utilized by man. They function by storing magnetic energy in the form of magnetic fields. These fields can interact with an external environment without actually doing any work on this environment, invoking the notion of a perpetual storage cell that never needs refueling. Furthermore, permanent magnets are the most efficient method of generating intense magnetic fields over short distances. Consider, for example, a modern permanent magnet 1 cm long emanating a field of 1 Tesla. To generate this same field, a 1 cm solenoid with wires 1 μm in diameter would have to carry a current of 1 Ampere!

Clearly then, the applications for permanent magnets are numerous, and they are in fact used extensively throughout industry as shown in Table 1.(1) The most important magnetic properties for general permanent magnet applications are the saturation magnetization, M_s (and consequently the remanent induction B_r), intrinsic coercivity H_c, energy product $(BH)_{max}$, and the Curie temperature T_c. Typical values of these parameters can be defined graphically in terms of a hysteresis plot, commonly referred to as a B-H loop, shown in Fig. 1. In this figure, B_r represents the residual magnetic induction in the material after the applied field has been removed, H_c represents the necessary field applied in the reverse direction to reduce the induction to zero, and $(BH)_{max}$ represents the maximum energy product contained in the second quadrant demagnetization curve of the hysteresis loop. As shown in Fig. 2,(2) there have been major improvements in magnetic properties of permanent magnets within the last twenty years, especially with the introduction of rare earth(RE) elements as an integral part of the alloy composition. Consequently, recently $(BH)_{max}$ values approaching 50 MGOe have been reported.(3) With such dramatic increases in $(BH)_{max}$, which defines the energy storing capacity of a permanent magnet, several new fields of applications for permanent magnets are being developed constantly. One such recent development is the "wiggler" used for generating synchroton radiation(4) and for weight savings applications in transportation, etc.

The coercivity and the energy-product(through its dependence on the coercivity, remanence and the shape of the hysteresis loop) both reflect the magnetization reversal process of the magnet. The harder it is to reverse magnetization in the magnet, the larger will be its H_c and

corresponding BH_{max}. Magnetization reversal can occur by two processes: the rotation of spins as shown in Fig. 3(a), or the nucleation and growth of reverse magnetic domains as shown in Fig. 3(b). Consequently, permanent magnets can be classified into single domain particle magnets and multi-domained magnets. In this paper the latter case will be focussed upon, since many technologically important magnets belong to this class.

In single domain particles, magnetization reversal occurs predominantly by the rotation of spins under large demagnetizing fields, fields on the order of the magnet's anisotropy field, H_K. H_K is defined as the field where the hard-axis magnetization approaches the easy-axis saturation magnetization value. Magnetization reversal occurring by uniform rotation of the spins sets the theoretical maximum value of the energy product for any permanent magnet. In multi-domained particles, magnetization reversal typically occurs by the nucleation and growth of reverse domains under demagnetizing fields much less than the anisotropy field. In this process, either the nucleation of reverse domains or the growth of these domains through domain wall motion can hinder magnetization reversal. Whichever event is more difficult for a particular magnet will control that magnet's reversal process, and this leads to a natural characterization of that magnet as a "nucleation-controlled" or "pinning-controlled" magnet. Characteristic virgin curves and hysteresis loops for a "nucleation controlled" and "pinning controlled" magnet are shown in Fig.4(a&b) respectively. Thus measurement of the virgin curve and the hysteresis loop is one of the main methods of distinguishing between the two classes of multi-domained magnets. Since H_c and $(BH)_{max}$ are structure and microstructure dependent, these properties can be manipulated by suitable modifications of the composition and processing, which in turn affect the microstructure and the magnetization reversal mechanism. Consequently, a critical step in improving $(BH)_{max}$ is the need to understand the relationship between the magnetization and demagnetization processes and microstructure. This understanding is crucial for designing the optimum microstructure for a particular magnet, as is schematically illustrated in Figs. 5(a-d). Fig. 5 (a) shows the typical microstructure of a Fe-Cr-Co elongated single domain permanent magnet.[7,9] This microstructure consists of a magnetic Fe-rich phase α_1, embedded in a paramagnetic Cr-rich phase α_2, both of which were formed by spinodal decomposition. This decomposition forms needle-shaped single domain particles of α_1, which can be aligned by the application of an applied field during the decomposition process, thus enhancing the magnetic induction. Magnetization reversal occurs by spin

rotation, which is prevented by the shape anisotropy of the particles. Consequently, high coercivity and the corresponding high $(BH)_{max}$ result from large aspect ratios, ratios on the order of four. As will be shown later in this paper, one class of Co-Sm alloys exhibits a two-phase cellular microstructure, Fig.5(b),typical of pinning type magnets.

A similar situation exists in the case of the precipitation hardened Fe-Cr-Co magnets, Fig.5(c). In this case, the domain walls are pinned by the Cr-rich α_2 particles and movement of the walls to reverse the magnetization can only occur by quantum jumps under strong magnetic fields. On the other hand, the recently developed Fe-RE-B alloys can be processed differently to give different structures. For example, in the case of sintered Fe-Nd-B magnets,(which will be discussed in detail later), the hard magnetic phase $Nd_2Fe_{14}B$ is surrounded by a paramagnetic Nd-rich phase at the grain boundaries, Fig.5(d). High coercivity and the corresponding high $(BH)_{max}$ result from the difficulty of nucleating reverse magnetic domains, which typically nucleate at grain boundaries. The Nd-rich phase serves to magnetically isolate the $Nd_2Fe_{14}B$ matrix grains, forcing each grain to nucleate its own reverse domain in order to reverse its magnetization. This in turn maximizes H_c and $(BH)_{max}$ for the whole particle aggregate magnet. Consequently, this microstructure is optimum for this particular reversal mechanism.[8]

As the above examples have shown, high H_c, high BH_{max}, and microstructural design go hand in hand. Microstructural design must take into account the relevant reversal process, and enhance magnetic properties by reducing microstructure features that facilitate that process. In nucleation-controlled magnets for example, the design objective is to minimize crystal defects that may serve as nucleation sites. Consequently, precipitates, dislocations, inclusions, etc. along with surface defects at the grain boundaries must be minimized. In contrast, the design objective for pinning type magnets is to maximize these defects. Therefore, microstructural design is an important consideration in permanent magnet materials.

The transition from single domain particle type magnets, such as Fe-Co-Cr to the present day magnets was made possible mainly due to the realization that the rare earth elements possessed not only large values of moments but also were capable of introducing giant magneto-crystalline anisotropies. Thus, by incorporating one or more of the rare earth elements of the lanthanide series to form a compound with low crystal symmetry (i.e., hexagonal or tetragonal), large values of magneto-crystalline anisotropy constants could be obtained. This fact,

along with the possibility of coupling the large moment of the rare earth elements parallel to the ferro-magnetic 3-d transition metal (Fe, Co, Ni) moment, meant that large values of saturation magnetization and remanence could be obtained in these rare earth -transition metal compounds. However, the existence of such desirable intrinsic magnetic properties alone cannot assure a good technical permanent magnet. The magnetic compound has to be processed into a bulk magnet with the optimum microstructure. This is the focus of this paper. In this paper, the microstructure of two of the main types of rare earth-transition metal based magnets will be discussed in their chronological order of development. Thus, in the next section, the microstructure of precipitation hardened Sm-Co based alloys will be discussed. Following this, the microstructural evolution of more recently developed Fe-Nd-B sintered magnets will be described which includes current research developments in the program at Berkeley.

B. THE Sm-Co TYPE MAGNETS

The discovery by Hofer and Strnat[20] that rare earth-transition metal compounds possess large values of magneto-crystalline anisotropy started the explosion of research on the structure, properties, microstructure and processing of such magnets. This was, however, stifled by the discovery of the Fe-Nd-B alloy system. However, the growing realization that the low Curie temperature (T_c= 312^{0}C) of $Nd_2Fe_{14}B$ and its correspondingly large temperature coefficient of induction impose severe limitations on the performance of permanent magnets based on this compound has created a resurgence of interest in magnets based on the Sm-Co system[10-13]. Because the Sm-Co magnets perform better at elevated temperatures and have greater tolerances for thermal excursions, it now seems that they will retain a market niche, even though it may be significantly reduced from what one would have projected in 1980, Fig.2. In the light of this renewed interest, it is appropriate to briefly review this class of alloys. Several other reviews are also available[14-19].

HISTORICAL DEVELOPMENT : After Hoffer and Strnat[20] first observed a large magnetocrystalline anisotropy in YCo_5 and Y_2Co_{17}, attention quickly focussed on $SmCo_5$ ($4\pi M_s$ = 9650 G, T_c = 724°C, and H_A = 210-290 kOe), and Sm_2Co_{17}($4\pi M_s$=12,000 G,T_c = 920°C, and H_A = 65kOe) as the two rare earth-transition metal compounds having the best combinations of these properties. These two compounds and a large array of analogous RE $(TM)_5$ and $(RE)_2$ $(TM)_{17}$ compounds are structurally related. The $SmCo_5$ phase has the $CaCu_5$ ($D2_d$) structure type with a primitive hexagonal lattice (P6/mmm) and one formula unit per primitive cell as shown schematically in Figure 6(a). The compounds of 2:17 stoichiometry are formed by ordered substitution of two Co atoms aligned along the c-axis at each of one third of the Sm sites; the two simplest orderings of these Co dumbells result in the hexagonal $(RE)_2$ $(TM)_{17}$ structure (Th_2 Ni_{17} type) favored by the heavy rare earths (Figure 6(b)) and the rhombohedral $(RE)_2$ TM_{17} structure (Th_2 Zn_{17} type) favored by the light rare earths including Sm (Figure 6(c)). In addition to these Co rich compounds, rare earth-transition metal systems commonly have compounds of 1:3 and 2:7 stoichiometries formed by ordered substitution of the rare earth at transition metal sites in the mixed planes. The close structural

similarities of these phases allow extensive mutual solid solubilities at elevated temperatures.

Based on its high anisotropy field, $SmCo_5$ has been widely used as a single phase permanent magnet. As such, its intrinsic coercivity, H_c, is limited by nucleation of reverse domains at grain boundaries, free surfaces and other discontinuities [21]. In practice, these single phase magnets are formed from powders, aligned and pressed in a magnetic field, then sintered in order to achieve a very high degree of crystallographic texture. Modifications to the $SmCo_5$ magnets include substitutions of Cu to promote a $SmCu_5$ - $SmCo_5$ decomposition product for domain wall pinning purposes and of Fe to raise the M_s [15].

Alloys based on stoichiometric Sm_2Co_{17} have the advantage of higher M_s but suffer from relatively low anisotropy. The anisotropy can be increased by substitutions of Fe, Mn, Zr, Hf, or Ti for some of the Co. By preferentially occupying the dumbbell sites in the 2:17 structures, these elements eliminate the major component of planar anisotropy, effectively strengthening the uniaxial anisotropy. In practice, the performance of stoichiometric 2:17 magnets is limited by nucleation of reverse domains at stacking faults and twin boundaries (See Figure7).

By shifting to compositions intermediate between 1:5 and 2:17 stoichiometry, a multiphase structure can be produced which combines the high M_s of the 2:17 compounds with domain wall pinning to maintain high coercivity. Alloys of this type have a "cellular" microstructure composed of a coherent distribution of rhomboid shaped 2:17 regions (~ 15nm in size) separated by continuous films (~ 10 nm thick) of the 1:5 phase [22-27]. Through a series of compositional and heat treatment modifications, alloys of this type have evolved which have energy products, $(BH)_{max}$, greater than 30MGOe. These alloys have compositions near Sm $(Co_{65}\ Fe_{21}\ Cu_{10}\ Zr_2)_{7.4}$ and must be homogenized at T = 1200°C, aged at T =850°C, then slowly cooled or step aged in order to develop the requisite microstructure [28, 29].

MICROSTRUCTURES : Four microstructural features are generally present in the Sm $(Co_{65}\ Fe_{21}\ Cu_{10}\ Zr_2)_{7.4}$ alloys aged to peak coercivity. A coherent cellular structure of :1) hexagonal 1:5 cell walls (~ 8 nm thick) and 2) rhombohedral 2:17 cell interiors (50-100 nm in size) is always observed. The R 2:17 particles occur in 3) two twin-related variants. 4) Occasionally superimposed on the cellular structure are thin platelets of a third phase.

Figures 8a and 8b show a TEM micrograph and associated electron diffraction pattern obtained from an alloy of this type. The cellular

structure is visible primarily through strain contrast; the R 2:17 twinning is visible as bands of alternating contrast running perpendicular to the common c-axis. The platelet phase is edge-on in this orientation and appears as narrow linear features running across the image from upper left to lower right. In these alloys, it is well known, e.g., by transmission electron microscopy xray microanalysis [27, 11, 12] that Cu segregates to the 1:5 cell walls and that Fe segregates to the 2:17 phase cell interiors. Zr is concentrated in the platelets and, to a lesser extent, in the 2:17 phase. Because the platelets are only observed in Zr-containing alloys, Zr seems to be a necessary constituent in them. The cellular structure is developed by aging treatments carried out at 850°C. Although the cell size does not change appreciably below 800°C, low temperature aging is necessary in order to partition the Cu and Fe among the major phases. It is believed [29] that the segregation of Cu to the 1:5 and Fe to the 2:17 has the effect of lowering the energy of a magnetic domain wall in the 1:5 phase compared to that in the 2:17 phase. This pinning of the domain walls in the 1:5 phase results in bulk hardening of these alloys (Figures 9 and 10).

The direct effects of the twinning of the R 2:17 and of the presence of the platelets on the macroscopic magnetic properties are not completely understood and may not be very significant. Both features lie parallel to the basal planes and perpendicular to the magnetic domain walls. Thus, a moving domain wall is expected to slide along the platelets and twin boundaries rather than encountering them directly. It should experience little resistance due to their presence. Rather, it has been argued [32] that the role of the platelets is indirect; they serve to enhance the kinetics of the Cu and Fe segregation. Alternatively, it has even been suggested [33] that the formation of the platelets may be detrimental; by providing a sink for Zr, the platelets eliminate any benefits Zr may give to the anisotropy of the R 2:17 phase [34]. In any case, these ideas must remain somewhat speculative because the actual crystal structure has not been worked out and is, in fact, a matter of some controversy [35, 36]. Because of their extreme thinness, the platelets in peak aged alloys do not form well defined electron diffraction maxima and so convergent beam analyses to identify the space group cannot be utilized. Through analysis of diffraction patterns obtained from extremely overaged platelets, their Bravais lattice has been determined [27] to be rhombohedral with a = 0.5 nm and c = 2.4 nm. Such a lattice is very similar to that of the Sm Co_3 phase, but the presence of Zr in the platelets means that the actual positions of the atoms within the unit cell differs from those in Sm Co_3

and probably involves some form of an ordered substitution of Zr in the 1:5 unit cell, but not at the Sm/dumbbell sites [33]. The structure of this phase has been imaged at high resolution and shows fringes corresponding to {0003} planes, Fig.11. Fidler et. al[35] have suggested that the platelets are hexagonal material. That this is not so can be proved by imaging using the following conditions : the electron beam along $[1210]_{1:5} \parallel [0110]_{R2:17} \parallel [1210]_{platelet}$. The (1015) planes do not occur in the H2:17 compound. Current work has in fact confirmed this inference and details will be published separately. However, a complete determination of the positions of the atoms within the unit cell will require synthesis of a bulk single crystal of the platelet phase and a full structure determination. A best guess at the composition of the plate might be Sm_4Zr_9 (Co Cu Fe)$_{25}$. Alternatively, atomic site imaging may resolve these constituents if a suitable thin foil can be prepared for atomic resolution electron microscopy.

EVOLUTION OF THE MICROSTRUCTURE : The remarkable uniformity of the cellular microstructure ultimately is a consequence of the instabilty of the R2:17 at T > 1150°C. Several authors have clearly demonstrated that the rhombohedral 2:17 phase with composition similar to that of the best permanent magnets undergoes one or more allotropic transformations at elevated temperature [10, 33, 37, 38]. For the compositions of interest here, the H2:17 modification is the stable form at T > 1150°C. During the usual quench-and-age treatment used to develop the cellular microstructure, the reverse transformation back to the R2:17 modification generates a high density of crystallographic defects; these defects serve as nucleation sites for precipitation of the 1:5 phase. The 1:5 particles grow to impingement along the pyramid planes because this is the orientation which seems to minimize elastic misfit energy [22]. The fact that the 1:5 nucleation is assisted by a phase change in the 2:17 parent phase also explains the high density of twins in the R2:17 material; the two twin-related variants are created in approximately equal numbers by the transformation from H2:17 to R2:17. Figures 12 and 13 show an example of an alloy, homogenized at 1200°C, then quenched. Prior to aging, a highly defective H2:17 is observed (Figure 12); after only 20 minutes at 850°C, a well-defined cellular structure is apparent (Figure 13).

The platelets begin to form in these materials well after the cellular structure is established. Figure 14 shows a plot of intrinsic coercivity as a function of aging time for alloys containing 1.5 and 3% Zr, with and without step aging. All alloys observed had the cellular structure; for 3%

Zr alloys the platelets did not form until 60 minutes into the aging sequence; 1.5% Zr alloys did not produce platelets until 4 hours aging. The platelets nucleate heterogeneously at the 1:5/2:17 interfaces or at grain boundaries and grow rapidly across the grain. Figure 15 shows a low Zr alloy overaged to the point of breakdown of coherency between the 1:5 and 2:17 phases. Some platelets extend across the interface; presumably they were present before loss of coherency. Other platelets terminate at the semi-coherent interface; they may have nucleated or been stopped by the interface. Because terminations of platelets show little strain contrast, it has been suggested [33] that they grow by a cooperative motion on alternating 1:5 basal planes of three mutually-cancelling dislocations, coupled with the diffusion of Zr to the leading edge of the platelet.

OUTSTANDING QUESTIONS AND DIRECTIONS FOR FURTHER DEVELOPMENT : Regarding the current generation of magnets, the outstanding questions center around the role(s) of Zr and of the platelet phase. That is, without a complete determination of structure and properties of the platelet phase, it is impossible to be confident as to what effect this phase has on the micromagnetics of these alloys. The next generation of magnets will probably only be produced through a radical re-design of the microstructures involved, changes being made based on insight gained from the microstructural studies of the current generation magnets. Finally, because the applications of these magnets will tend to be concentrated in areas where elevated temperatures are a concern, further efforts should be expended in developing the use of heavy rare earth substitutions for temperature compensation.

Zr has at least 5 metallurgical effects in these alloys [10, 27]. It inhibits Sm diffusion, slowing cell growth. It seems to modify the misfit between 1:5 and 2:17, encouraging regularity and uniformity of the cellular structure. The presence of Zr increases the degree of segregation of Cu to 1:5 and Fe to 2:17 and stabilizes the platelets, leading to increased transport rates. Finally, Zr stabilizes the H2:17 at high temperature. The questions remaining regarding Zr center around its relation to the platelet phase. First of all, what is the structure of the platelet; is it possible that it is a pseudo-ternary compound with excellent permanent magnet properties of its own? If not, would the overall magnet be improved if Zr could be retained in the R2:17 where it is known [39] to favorably influence magnetocrystalline anisotropy? Because Zr plays so many roles, it is conceivable that other elements (e.g. Nb, Hf, Ti . . .) could be found which play some of Zr's functions and not others; could they be

manipulated to truly optimize all of these phenomena? A simple calculation [40] suggests that the maximum energy product for a Sm_2 (Co Fe Mn)$_{17}$ alloy could theoretically be as high as 49 MGOe, a factor of 1.5 times that of the current generation of magnets. Thus, there is ample reason to believe that further improvements may be possible. The practical challenge lies in designing a high coercivity microstructure without sacrificing saturation magnetization by adding excessive amounts of Cu, Zr or other non-ferromagnetically coupled species. Based on observations of the current generation magnets, one might envisage an optimized microstructure having a small volume fraction of Cu-rich 1:5 in the form of widely separated, 8 nm thick, sheets parallel to the c-axis of a high anisotropy, high magnetization R 2:17. To generate this microstructure, the Cu content must be reduced significantly while maintaining H 2:17 stabilization at high temperature. Morita et al. [10] have shown that this is possible in the presence of Zr; one can only speculate whether other elements might be more effective. To align the 1:5 parallel to the c-axis of the R 2:17 compositional modifications should be sought which create a larger mismatch along "a", but a smaller mismatch along "c". Hf additions have potential here; alloys containing this element have cell walls significantly closer to the c-axis [41] than do the Zr-containing alloys.

By substituting heavy rare earths for Sm in the 1:5 and 2:17 compounds it is possible to reduce the dependence of their properties over a range of temperatures [42-44]. While this has been known for sometime, very little work of this type has been done on the precipitation hardened magnets. More effort should be expended in this area in order to design magnets which perform well in the range $200 < T < 400^{o}C$ where a market niche still remains.

However, for room temperature applications, the Sm-Co system has to compete with the Fe-Nd-B class of magnets.

In the next section, the microstructural details and some aspects of magnetization reversal of the Fe-Nd-B class of magnets will be reviewed.

C. MICROSTRUCTURE AND MAGNETIC PROPERTIES OF SINTERED Fe-Nd-B MAGNETS

In sintered permanent magnets, such as Fe-Nd-B, magnetization reversal occurs by the nucleation and movement of domain walls in the grains of the polycrystalline magnets(45). Because of such a domain wall process, the intrinsic coercivity, iHc, (or the nucleation field, H_n) is much lower than the anisotropy field of the magnetic phase. For example, in the case of Fe-Nd-B magnets, the room temperature anisotropy field, $2K_1/M_s$, of the magnetic phase, $Nd_2Fe_{14}B$, is 71kOe, while the best value of room temperature iHc is only about 12-14kOe(46). This is also true in the case of $SmCo_5$ magnets(47). This difference is due to the fact that in such polycrystalline magnets, wherein the magnetocrystalline anisotropy of the magnetic phase is very high (which is the cause for uniaxial magnetization and a large value of anisotropy field), there exist regions of considerably lowered anisotropy. This in turn means that at these regions, it is potentially more favorable for the magnetization to reverse, by the nucleation of a domain wall. Examples of such regions are grain boundaries, two-phase interfaces, incoherent precipitate-matrix interfaces, anti-phase domain boundaries, strained regions, etc. The magnetocrystalline anisotropy of such regions can be reduced either due to the structural heterogeneity of the region or due to differences in the chemical nature of the region and its neighborhood. A variety of sintered Fe-RE-B magnets are being investigated in our research program, not only to understand the structure-property relationships in this class of magnets, but also to study the effect of alloying additions on the microstructure and magnetic properties of the magnets. The magnets being studied have similar overall compositions consisting of Fe-(34-36) wt.% rare earth-1 wt.% B. Their general microstructure is two-phase : the ferromagnetic tetragonal $Nd_2Fe_{14}B$ phase, Fig.16(a)(49), surrounded by a complex paramagnetic rare earth rich, oxygen stabilized phase at the grain boundaries. These general microstructural details are summarized in Fig.16(b).

Consequent to the discovery of this alloy system(46,48,49), it has been intensively researched by several research groups around the world in order to understand the nature of magnetization reversal, both in the sintered magnets as well as in the melt spun magnets. The latter aspect is dealt with in a separate paper(50). Through the results of the intensive experimentation, it has been firmly established that the magnetization reversal in sintered magnets is controlled by the wall nucleation step, i.e.,

the magnet has been termed a "nucleation controlled" magnet. However, the exact cause of wall nucleation is still not understood, although it is generally accepted that the nucleation event is most likely to occur at the grain boundaries and the interphase interfaces.

MICROSTRUCTURE : Experimental evidence is now well established for the existence of a Nd-rich phase at the grain junctions that frequently extends into the two-grain boundaries as thin layers of about 200-500Å thickness[8,51-57]. The structure of this phase and its composition has been determined by micro-diffraction and analytical electron microscopy(AEM), as summarized in Figs.16(b) and 17. It must be pointed out that specimen preparation for TEM is a non-trivial problem and great care is necessary to avoid artefacts and specimen damage by ion-beam thinning. By small probe analysis, i.e., microdiffraction, the structure of the phase at the grain boundaries was found to be fcc in all cases. Microanalysis was carried out using an ultra-thin window energy dispersive x-ray detector fitted to a JEOL 200CX electron microscope. The low energy end of the EDX spectrum from the grain boundary phase is shown in Fig.16(b) (top left corner). An important aspect of the spectrum is the fact that in all the cases, a definite oxygen peak is observed. Quantification using experimentally determined k-factors for oxygen yielded oxygen contents of upto 40 at.%. This explains the fcc structure observed since two fcc Nd oxides are known to exist[58]. Oxygen can enter the system during any of the various processing steps. The possible effect of oxygen on the magnetization reversal process will be alluded to later. Although the presence of oxygen in the grain boundary phase was first suggested by Stadelmaier and co-workers it has been only experimentally verified by AEM[51]. The presence of oxygen was independently verified by Auger spectroscopy and elemental mapping. This was carried out using an in-situ fractured sample. The fracture surface consists of a mixed inter-granular and trans-granular fracture, as shown in Fig.18(a). In Figs.18(b) and (c), the oxygen and Nd Auger electron maps are shown. The similarity in the intensity distribution of the two maps clearly indicates that oxygen and Nd occur together, in the grain boundary phase.

In several cases, the fcc region, especially in the grain junctions, exhibits ordering. This is indicated by the observation of extra spots in the selected area diffraction patterns(SAD). One typical example is shown in Fig.19. In this figure, a large region of the fcc phase is shown in the bright field image. The four insets show zone axis SAD patterns in four fcc zones. The extra spots in the diffraction patterns indicate ordering, possibly of the oxygen atoms. However, this does not appear to correlate

with changes in the magnetic properties of the magnet upon post-sintering heat-treatment, since the extra spots appear in both the as-water quenched magnet as well as in the optimally treated magnet.

In addition to these two features , a third phase of composition close to $Fe_4Nd_{1+x}B_4$ is observed as a minority phase (about 5 vol.%)[46,47] as well as the rare earth sesqui-oxide[53]. However, the latter two are not of great importance in determining the magnetic properties nor the changes in the magnetic properties with thermal treatments, and hence will not be considered further.

One particular aspect of the microstructure which is of great significance in understanding the magnetization reversal mechanism is the interface between the matrix $RE_2Fe_{14}B$ phase and the grain boundary fcc phase. This has been examined by several workers and there has been considerable debate about the exact nature of the microstructural features that are responsible for the nucleation of domain walls that cause magnetization reversal[51-57,60-63]. Specifically, the discussion has centered around the fact that a water quenched magnet shows low intrinsic coercivity, iHc, of about 3-4 kOe[48]. If the water quenched magnet is annealed at temperatures of 500-600°C for an hour, the iHc increases sharply to a high value of about 10-11 kOe. Alternately, a high iHc value comparable with that of the annealed magnet, can be obtained if the magnet is slowly cooled from sintering temperature (50°C/hour)[64].

In the original work of Sagawa et. al[46,48] it was suggested that the annealing treatment relieved quenching stresses and smoothed the grain boundaries and two phase interfaces. Hiraga et. al[60,61], through high resolution TEM proposed that in the water quenched condition, the matrix $RE_2Fe_{14}B$ phase was penetrated by bcc platelets from the grain boundary regions. This phase was reported to have a Fe:Nd ratio similar to that of the matrix phase, with a lattice parameter close to that of bcc Fe. Tokunaga et. al[57] also observed the bcc platelets, but did not note any correlation between the density of platelets and the coercivity. Sagawa et. al[65] produced, by melt spinning, an Fe-Nd phase which they suggested was equivalent to the grain boundary bcc phase observed by Hiraga et. al[60,61]. This phase had a Curie temperature of 150°C. Livingston[55] has countered this suggestion with the argument that if a large atom such as Nd were to dissolve in Fe, considerable changes in the lattice parameter of the bcc phase should be observed, which is not the case. Also, if the Curie temperature of this phase is 150°C, increased wall pinning above 150°C should be expected. However, this has not been observed.

Stadelmaier and co-workers[59,62] have suggested that the grain boundary phase consists of a fine dispersion of Fe in a glassy oxide phase formed during cooling. It has, however been shown by the present authors that the bcc phase observed could arise due to ion milling artefacts. Moreover, it has been observed by HREM that the interface between the matrix and the grain boundary phase is devoid of any other phase. This is true of the water quenched magnet as well as the quenched and annealed magnet. Fig.20(a) depicts a HREM image of one such interface in the water quenched magnet, while the corresponding interface in the annealed magnet is shown in Fig.20(b). Both magnets were prepared from the same starting alloy and were sintered under identical conditions. It is noteworthy that in neither of the images a third phase at the interface is observed although the structure is not perfect all along the boundary. Thus, the changes in magnetic properties with post-sintering annealing appears to be caused by some other changes in the microstructure or local composition.

Magnetic measurements have shown that the general behaviour of the quenched, slowly cooled and the quenched and annealed magnets are similar[46,48,66-69]. For example, all of them behave as nucleation type magnets, with a large value of virgin permeability. The main difference between them is the fact that nucleation occurs at lower fields in the water quenched magnets as compared to the slowly cooled magnets. One aspect that may be of importance in explaining the changes in magnetic properties is the stress developed in the magnet due to quenching. Specifically, stresses due to differences in the thermal expansions of various phases in the multi-phase magnet may lead to significant reductions in the overall anisotropy of magnetization. The matrix $RE_2Fe_{14}B$ phase has been shown to have anisotropic thermal expansions along the c-axis and the a-axis. In addition, there is bound to be a difference in the thermal expansivity of the matrix phase along the a-axis, and that of the grain boundary fcc phase. Thus, stresses at the matrix phase-fcc phase interface can arise due to thermal expansion mismatch. In addition, the high cooling rate of the water quench can exacerbate the situation by not permitting relaxation of the stresses by diffusive creep. The stresses at the interfaces coupled with the rather large value of spontaneous magnetostriction of the $RE_2Fe_{14}B$ phase[70] suggests that in the water quenched magnet, a significant contribution due to stress anisotropy has to be taken into account.

Scanning electron microscopy of the quench cracked surface clearly indicates that the fracture is almost completely inter-granular. This is shown in Fig.21(a), while the magnified image of (a) is shown in (b). This

again supports the idea that quenching stresses manifest at the grain boundaries and two phase interfaces. It is also conceivable that the presence of oxygen at the grain boundaries is responsible for inter-granular embrittlement. This phenomenon is very common in ferrous alloys. Hence the combined effect of oxygen induced embrittlement and quenching stresses not only leads to inter-granular fracture, but more importantly, a large decrease in the magnetocrystalline anisotropy close to the interfaces. This, again explains, albeit qualitatively, why the coercivity is much smaller than the anisotropy field, even in the case of the slowly cooled magnet. In this case, the presence of oxygen at the grain boundaries and interfaces, is likely to reduce the magnetocrystalline anisotropy of the matrix phase, close to the interfaces. Jin et. al[71] have examined the effect of point defects upon the magnetocrystalline anisotropy of the rare earth sub-lattices in the case of $SmCo_5$ magnets. They have found that a considerable decrease in the magnetocrystalline anisotropy can be brought about if certain of the rare earth atoms are removed from the sub-lattice. A similar phenomenon could be occurring in the case of $Nd_2Fe_{14}B$, wherein, the electronic configuration of the Nd sub-lattices could be modified considerably by the presence of oxygen in the neighborhood, such that the large contribution to the magnetocrystalline anisotropy by the Nd sub-lattice is substantially reduced. However, this idea has to be further validated by calculations similar to that of Jin et. al. The lower iHc than that of the slowly cooled magnet can be attributed to the fact that in the case of the water quenched magnet the effect of stresses add up with the effect of oxygen (which can be considered as one of the defects that can cause domain wall nucleation). The effect of quenching rate (and hence quenching stresses) on the iHc and the energy product, $(BH)_{max}$ can be studied by measuring the magnetic properties of magnets cooled at different rates from the sintering temperature[73]. Fig.22 shows a plot of intrinsic coercivity and energy product against cooling rate. It can be clearly seen that the cooling rate from the sintering temperature has a pronounced effect on the intrinsic coercivity and hence on the energy product. This marked influence of the cooling rate from the sintering temperature suggests that the quenching stresses may play an important role in the nucleation of domain walls at the grain boundaries. This aspect needs to be further examined in order to better understand the combined effect of magneto-crystalline anisotropy and quenching stresses in the presence of a large value of spontaneous magnetostriction.

EFFECT OF ALLOYING ADDITIONS : Although the Fe-Nd-B alloy system

has shown considerable promise, there are some debilitating aspects, that can prevent wide ranging applications of this magnet. Prime among them is the fact that the Curie temperature is quite low, when compared to that of Sm-Co magnets. This in turn leads to a rapid fall in the intrinsic coercivity with temperature, i.e., a high temperature coefficient of iHc. Consequently, normal demagnetizing fields can cause large irreversible losses of magnetization. In addition, the low Curie temperature leads to a high reversible temperature coefficient of remanence. Thus, the two important permanent magnet characteristics are strongly influenced by the low Curie temperature. To overcome this, alloying additions have been resorted to. The Curie temperature can be raised by the addition of Cobalt. However, this lowers the iHc, which can be compensated for by the addition of Al or even better Dy. The strong similarity in the chemical properties of the rare earths makes it easier to replace one by another. Thus, for example, Nd has been replaced by Dy in the $RE_2Fe_{14}B$ lattice in order to take advantage of the large anisotropy contribution of Dy (the anisotropy field of $Dy_2Fe_{14}B$ is reported to be 159kOe). However, Dy couples anti-parallel to the Fe sub-lattice magnetization, leading to a decrease in the remanence. Through Dy additions it has been possible to achieve iHc values in the range of 25kOe, along with a remanence of about 8-9kG. However, the energy product in this case is not very high. It has also been shown that high iHc values can be obtained by the addition of Al, which replaces Fe, thus lowering the remanence of the magnet. These aspects have been reviewed by Livingston(55) . Okada and co-workers(64) have shown that replacement of Nd by an alloy of Ce-Pr-Nd (didymium) can reduce the cost of production of the magnets. However, the magnetic properties are inferior to that of the ternary Fe-Nd-B magnet.

One of the aspects that requires more attention is the effect of such alloying additions upon the microstructural and micro-analytical details of the magnet. For example, it would be of great significance to know whether the additive is uniformly distributed among the various phases in the magnet, preferentially partitions to one of the phases,or is segregated to the inter-phase interfaces, as illustrated schematically in Fig.23. In this figure, the concentration of the alloying element is plotted as a function of distance from the fcc phase-matrix interface. It shows a strong segregation of the alloying element to the interfaces. If the segregating element is, for example, Dy (which has a large value of magnetocrystalline anisotropy), then a large local increase in the anisotropy field of the $RE_2Fe_{14}B$ phase can be expected. Microanalytical

information about substitutionally alloyed magnets is even more important since the magnetization reversal is controlled by wall nucleation at the interfaces. The segregation (or de-segregation) of the additive element may significantly alter the nucleation field for magnetization reversal. Clearly, a correlation of the microstructure and micro-chemical details of the substituted magnet to the magnetic properties obtained would assist in the design of specific microstructures to optimize the different related magnetic properties. Such studies are just beginning in the case of the Fe-Nd-B alloy system[54,72]. It is equally important to determine any propensity for specific site occupancy, of the substituent species, since both the $Nd_2Fe_{14}B$ unit cell and the Sm_2Co_{17} unit cell contain more than one sub-lattices, all of which do not have the same characteristics. Indeed, in the case of Sm_2Co_{17} the technique of channelling enhanced xray microanalysis using a transmission electron microscope, has been invaluable in determining the specific site ocupancies of substituent species[74, 75]. It is likely that the application of such a technique in the case of the Fe-Nd-B magnets will enable the optimization of the concentrations of the substituent atoms.

SUMMARY

In this paper an attempt has been made to review and identify the major microstructural and microanalytical constituents of C0-Sm and Fe-Nd-B magnets which are differ fundamentally in their magnetization reversal mechanism. From these observations some suggestions for future directions are outlined.

ACKNOWLEDGEMENTS

This work is supported by the Director, Office of Energy Research, Office of Basic Energy Sciences, Division of Materials Science of the U.S.Department of Energy under contract No. DE-AC03-76SF00098

REFERENCES

1. McCaig,M.,Permanent Magnets in Theory and Practice, Halsted Press, New York;1977.
2. R.M.White,Science, 229 #4708, 11-15 July 5, 1985.
3. K.S.V.L.Narasimhan, Jl. of Appl. Phys., 57, 4081,(1985).
4. Lawrence Berkeley Laboratory Technical Information Department.
5. J.J. Becker. IEEE Trans. on Mag., Mag-12, No.6, 965, (1976).
6. L. Rabenberg, R.K.Mishra and G.Thomas, Jl. of Appl. Phys. 53, 2389, (1982).
7. Y.Belli, G.Thomas, M.Okada, M.Homma, H.Kaneko, Jl. of Appl. Phys., 49, 2049, (1978).
8. R.K. Mishra, J.K.Chen and G.Thomas, Jl. of Appl. Phys. 59 ,2244, (1986).
9. M.Okada, M.Homma, H.Kaneko and G.Thomas, IEEE Trans. on Mag., Mag.-14, 245, (1978).
10. Y. Morita, T. Umeda and Y. Kimura, Paper DC-01 in the 1987 Intermag Conference, Tokyo,April 1987. To appear in IEEE Trans. Magn.
11. Y. Fukui, T. Nishio and Y. Iwama, Paper DC-02 in the 1987 Intermag Conference, Tokyo,April 1987. To appear in IEEE Trans. Magn.
12. K. Morimoto, M. Watanabe and T. Takeshita, Paper DC-03 in the 1987 Intermag Conference, Tokyo, April 1987. To appear in IEEE Trans. Magn.
13. A. E. Ray, W. A. Soffa, J. R. Blachere and B. Zhang, Paper DC-04 in the 1987 Intermag Conference, Tokyo, April 1987. To appear in IEEE Trans. Magn.
14. J. Fidler, Proceedings of the Fifth International Workshop on Rare Earth - Cobalt Permanent Magnets and Their Applications; Roanoke, VA, (1981).
15. E. A. Nesbitt and J. H. Wernick, Rare Earth Permanent Magnets, (Academic Press, New York, 1973).
16. W. E. Wallace and K. S. V. L. Narasimhan in Science and Technology of Rare Earth Materials, E. C. Subbarao and W. E. Wallace, Eds.,(Academic Press, New York, 1980).

17. K. P. Gupta in Science and Technology of the Rare Earth Materials, E. C. Subbarao and W. E. Wallace, eds., (Academic Press, New York, 1980).
18. G. Asta and A. Deriu in Proceedings of the Sixth International Workshop on Rare Earth-Cobalt Permanent Magnets and Their Applications, J.Fidler, ed., (Druckerei Lischkar and Co., Vienna, 1982).
19. W. E. Wallace, H. Fujii, M. V. Satyanarayana andS.Hirosawa,Proceedings of the Sixth International Workshop on Rare Earth-Cobalt Magnets and Their Applications, J. Fidler, ed., (Druckerei Lischkar and Co., Vienna, 1982).
20. G. Hoffer and K. Strnat, IEEE Trans. Magn. MAG.-2 487, (1966).
21. J. D. Livingston, Phys. Status Solidi, A18, 579 (1973).
22. J. D. Livingston and D. L. Martin, Jl. of Appl. Phys., 48, 1350, (1977).
23. J. D. Livingston, IEEE Trans. Magn. MAG-14, 668 (1978).
24. K. N. Melton and H. Nagel, J. Appl. Phys., 47, 2671 (1976).
25. T. Yoneyama, A. Fukuno and T. Ojima, Proceedings of the Fourth International Conference on Rare Earth-Cobalt Magnets and Their Applications, Japan, 407, (1979).
26. R. K. Mishra and G. Thomas, Proceedings of the Fourth International `Workshop on Rare Earth-Cobalt Magnets and Their Applications, 301 (Hakone, Japan, May 1979).
27. L. Rabenberg, R. K. Mishra and G. Thomas, Jl. of Appl. Phys., 53, 2389,(1982).
28. T. Ojima, S. Tomizawa, T. Yoneyama and T. Hori, IEEE Trans. Magn.,MAG-13, 1317, (1977).
29. R. K. Mishra, G. Thomas, T. Yoneyama, A. Fukuno and T. Ojima, Jl. of Appl. Phys., 52, 2517 (1981).
30. A. E. Ray, Jl. of Appl. Phys., 55, 2094, (1984).
31. H. Nagel, Jl. of Appl. Phys., 50, 1026, (1979).
32. L. Rabenberg, R. K. Mishra and G. Thomas, Proceedings of the Sixth Annual Workshop on Rare Earth-Cobalt Permanent Magnets and Their Applications, Vienna, 599-608, Sept., 1982.
33. L. Rabenberg, Ph.D. Thesis University of California, Berkeley, 1983. (Available through University Microfilms, Ann Arbor, MI).
34. M. V. Satyanarayana, H. Fujii and W. E. Wallace, Jl. of Appl. Phys., 53, 2374, (1982).
35. J. Fidler, P. Skalicky and F. Rothwarf, IEEE Trans. Magn., MAG-19, 2041, (1983).
36. L. Rabenberg, R. K. Mishra and G. Thomas, IEEE Trans. Magn., MAG-19,

2723, (1983).

37. Y. Khan, Acta Cryst., B30, 1533, (1974).
38. M. Sahashi, T. Mizoguchi, K. Inomata, J. Mag. Magn. Mat., 31, 225, (1983).
39. Ying-chang Yang, Hai-ying Chen, Feng Xing, Wen-wang Ho, Peng Wu, Ji-Lian Yang, Bai-shen Zhang, Hui-ming Zhou, Lan Jin, Jhi-jiang Xu,Xiang-xin Zeng, IEEE Trans. Magn. MAG-21, 1987 (1985).
40. H. Zijlstra, IEEE Trans. Magn. MAG-14, 661, (1978).
41. J. Fidler and P. Skalicky, J. Mag. and Magn. Mat., 27, 127, (1982).
42. K.S.V.L. Narasimhan, M.G.H. Wells and D.V. Ratnam, Jl.of Appl. Phys., 49, 2072, (1978).
43. F. G. Jones and M. Tokunaga, IEEE Trans. Magn., MAG-12, 968, (1976).
44. C. J. Willman and K.S.V.L. Narasimhan, IEEE Trans. Magn., MAG-21, 1976, (1985).
45. J.D.Livingston, Paper No. AC-06, Intermag-1987, Tokyo, Japan, April 14-18,1987.
46. M.Sagawa, S.Fujimura, H.Yamamoto, Y.Matsuura and K.Hiraga, IEEE Trans. Magnetics, Mag-20, 1584-1589, (1984).
47. J.D.Livingston, AIP Conf. Proc. 10, 643, (1973).
48. M.Sagawa, S.Fujimura, N.Togawa, H.Yamamoto and Y.Matsuura, Jl. of Appl. Phys., 55, 2083-2087, (1984).
49. J.F.Herbst, J.J.Croat, F.E.Pinkerton and W.B.Yelon, Phys. Rev., 29B, 4176-4178, (1984).
50. R.K.Mishra,Present Symposium Proceedings.
51. R.Ramesh, J.K.Chen and G.Thomas, Jl. of Appl. Phys., 61, 2993-2998, (1987).
52. J.Fidler and L.Yang, in Proc. Eighth Int. Workshop on Rare Earth Permanent Magnets and their Applications, Ed. K.J.Strnat, University of Dayton Press, 647, (1985)
53. R.Ramesh, K.M.Krishnan, E.Goo, G.Thomas, M.Okada and M.Homma, Jl. of Mag. and Magn. Matls., 54-57, 563-567, (1986).
54. R.Ramesh, G.Thomas and B.M.Ma, Proc. Symposium on Permanent Magnetic Materials, MRS Spring Meeting , Anaheim, Ca, (April 21-25, 1987).
55. J.D.Livingston, in Proc. ASM Symp. on Soft and Hard Magnetic Materials, Eds. J.A.Salsgiver et. al., Florida, 71-79 ,(4-9 October 1986).
56. P.Schrey, IEEE Trans. on Magnetics, Mag.-22, 913-915, (1986).
57. M.Tokunaga, M.Tobise, N.Meguro and H.Harada, IEEE Trans. on Magnetics, Mag.-22, 904-909, (1986).

58. K.A. Gschneidner, Rare Earth Alloys, Van Nostrand Publishing Co., Princeton, NJ., (1961).
59. H.H.Stadelmaier and N.A.El Masry, in Proc. Eighth Int. Workshop on Rare Earth Permanent Magnets and their Applications, Ed. K.J.Strnat, University of Dayton Press, 613-634, (1985).
60. K.Hiraga, M.Hirabayashi, M.Sagawa and Y.Matsuura, Jap. Jl. of Appl. Phys., 24, L30-32, (1985).
61. K.Hiraga, M.Hirabayashi, M.Sagawa and Y.Matsuura, Jap. Jl. of Appl. Phys., 24, 699-703, (1985).
62. N.A.El Masry and H.H.Stadelmaier, Materials Letters, 3, 405-408, (1985).
63. J.Fidler, IEEE Trans. on Magnetics, Mag.-21, 1955, (1985).
64. M.Okada, S.Sugimoto, C.Ishizaka, T.Tanaka and M.Homma, Jl. of Appl. Phys., 57, 4146, (1985).
65. M.Sagawa, S.Hirosawa, H.Yamamoto, Y.Matsuura, S.Fujimura, H.Tokuhara and K.Hiraga, IEEE Trans. on Magnetics, Mag.-22, 910-912, (1986).
66. J.Schneider, R.Grossinger, R.Krewenka, U.Heincke and H.Sassik, Materials Letters, 3, 401-404, (1985).
67. M.Sagawa, S.Fujimura, H.Yamamoto, Y.Matsuura, S.Hirosawa and K.Hiraga, Proc. Eighth Int. Workshop on Rare Earth Permanent Magnets and their Applications, Ed. K.J.Strnat, University of Dayton Press, 587-612, (1985).
68. K.D.Durst and H.Kronmuller, Proc. Eighth Int. Workshop on Rare Earth Permanent Magnets and their Applications, Ed. K.J.Strnat, University of Dayton Press, 725-736, (1985) .
69. K.D.Durst and H.Kronmuller, Jl. of Magn. and Mag. Matls., 68, 63-75, (1987).
70. A.V.Andreev, A.V.Deryagin, S.M.Zadvorkin and S.V.Terent'ev, Sov. Phys. Solid State, 27, 987,(1985).
71. H-M.Jin, H-N.Chen, D-S.Tang, J-F.Han and S.Yen, in Proc. of the Sixth Int. Workshop on Rare Earth Permanent Magnets and their Applications, Ed. J.Fidler, Technical University of Vienna, 549-554, (1982).
72. J.K.Chen and G.Thomas, in Proc. of Symp. on Permanent Magnetic Materials, MRS Spring Meeting, Anaheim, Ca, (21-25 April, 1987).
73. R.Ramesh, G.Thomas, M.Okada and M.Homma, Paper No.AC-07, Intermag-1987, Tokyo, Japan April14-18 1987.
74. K.M.Krishnan, L.Rabenberg, R.K.Mishra and G.Thomas, Jl. of Appl. Phys., 55, 2058-2060, (1984).

75. K.M.Krishnan, " Atomic site and species determinations using channelling and related effects in Analytical Electron Microscopy,"Ultramicroscopy, Special publication entitled "Limits of sub-micron-microscopy", Eds. J.J.Hren and M.J.Kersker, in press.

Figure 1 A typical B-H plot showing the virgin magnetization curve, hysteresis loop and the parameters B_r, H_c and $(BH)_{max}$.

Figure 2 Historical trend of the maximum energy product, $(BH)_{max}$ and intrinsic coercivity, H_c, since the year 1900.

Figure 3 Magnetization reversal mechanisms in permanent magnets : (a) uniform rotation of spins in single domain particles ; (b) nucleation and growth of domain walls to reverse the magnetization in multi-domained magnets.

Figure 4 Typical virgin curves and hysteresis loops for : (a) a nucleation controlled magnet ; (b) a pinning controlled magnet.

Figure 5 A schematic illustration of different types of microstructures generally observed in permanent magnets : (a) typical microstructure of Fe-Cr-Co elongated single domain particle magnet ; (b) precipitation hardened Fe-Cr-Co alloys, showing the Cr-rich particles at which the domain wall is pinned; (c) two-phase cellular microstructure of Sm-Co magnets ; (d) typical microstructure of a sintered Fe-Nd-B magnet.

Figure 6(a) Perspective drawing of the $SmCo_5$ conventional unit cell ; (b) Perspective drawing of the hexagonal Sm_2Co_{17} primitive unit cell. This structure is formed by ordered substitution of dumbbell pairs of Co at one third of the Sm sites. The corresponding primitive cell of the $SmCo_5$ is outlined ; (c) Perspective drawing of the rhombohedral Sm_2Co_{17} primitive unit cell formed by an ordered substitution of pairs of Co atoms at Sm sites; the corresponding $SmCo_5$ primitive cell has again been outlined.

Figure 7 Transmission electron micrograph of stacking faults in a stoichiometric 2:17 magnet.

Figure 8 Typical Image and SAD of cellular structure. The cell walls are imaged primarily due to strain contrast. The twins in the R2:17 are visible as bands of light and dark contrast perpendicular to the c-axis. The platelets are the linear features running from upper left to lower right. The SAD and indexing are consistent with a combination of 1:5 and twinned rhombohedral 2:17 structures. The intense spots are common to

all phases; the weaker spots are from the two variants of the R2:17, only one of which has been explicitly indexed. An extra spot at 0.8 inverse nanometers along (0001)* is the only distinct reflection from the platelet phase. (3wt% Zr alloy; 1 hour at 850°C; step-aged).

Figure 9 Schematic drawing of a domain wall in the cellular structure, showing pinning of the wall to the 1:5 phase.

Figure 10 Lorentz electron micrograph of magnetic domain walls in a precipitation hardened $Sm(Co\ Cu\ Fe\ Zr)_{7.4}$ magnet.

Figure 11 High Resolution TEM image of the platelet phase with the {0003} planes being imaged.

Figure 12 BF and DF of a homogenized and quenched alloy. The upper BF image shows what appears to be a clean, single-phase structure; the lower DF image using the streak shows the presence of some heterogeneities in the foil. The SAD indicates that this foil is almost completely H2:17. (1.5 wt % Zr alloy; 1 hour at 1200°C; quenched).

Figure13 BF image and SAD pattern of a homogenized, quenched, and aged specimen, showing a well-defined cellular structure. (1.5 wt% Zr alloy; 1 hour at 1200°C; quenched; 20 minutes at 850°C).

Figure 14 Intrinsic coercivity as a function of aging time and platelet nucleation. Alloys were aged at 850°C for times given on the x-axis, then quenched. Some alloys were subsequently step-aged. The X's in the figure correspond to the time at which the platelets form.

Figure 15 BF and weak beam dark field images of a 1:5 cell wall which has lost coherency. The fact that several platelets terminate at the 1:5/R2:17 interface indicates that this may be a preferred nucleation site. (1.5 wt %Zr alloy; 40 hours at 850°C).

Figure 16 (a) Schematic illustration of the unit cell of $Nd_2Fe_{14}B$, showing the atomic positions in the six Fe- sub-lattices, two Nd sub-lattices and the boron atom positions ; (b) compound illustration showing the Nd-rich, oxygen stabilized, fcc phase at the triple junctions and the grain boundaries of the $Nd_2Fe_{14}B$ phase. The low energy end of the

EDX spectrum (top left corner) shows the oxygen peak while the tableau of diffraction patterns confirms the fcc structure.

Figure 17 Bright field image of a thin strip of the grain boundary phase along with the nano-probe diffraction patterns in the [110] zone axis orientation, confirming the fcc structure.

Figure 18 Fractograph of an in-situ fractured Auger sample of an optimally treated Fe-Nd-B magnet ; (b) Oxygen Auger electron map corresponding to the region depicted in (a) ; (c) Nd Auger electron map corresponding to the region shown in (a). Note that the regions of high intensity in (b) correspond to regions of high intensity in (c).

Figure 19 Bright field micrograph of the Nd-rich phase in a typical Fe-Nd-B magnet along with the SAD pattern in the [100] zone axis orientation showing the presence of ordered spots. (Sample slowly cooled from sintering temperature).

Figure 20 (a) Lattice fringe image of the interface between the matrix $Nd_2Fe_{14}B$ phase and the grain boundary Nd-rich phase in a water quenched Fe-Nd-B magnet showing the absence of any other phase between these two phases ; (b) lattice fringe image of a similar interface in the case of an annealed magnet, again showing the absence of any other phase.

Figure 21 (a) Scanning electron micrograph of the quench cracked surface in a water quenched typical Fe-Nd-B magnet showing inter-granular fracture ; (b) a magnified image of the micrograph shown in (a).

Figure 22 A plot of intrinsic coercivity and energy product against the cooling rate for a typical Fe-Nd-B magnet.

Figure 23 A schematic plot of the concentration of the alloying element as a function of distance from the fcc phase-matrix phase interface in a Fe-Nd-B magnet, showing a strong segregation of the alloying element to the interfaces.

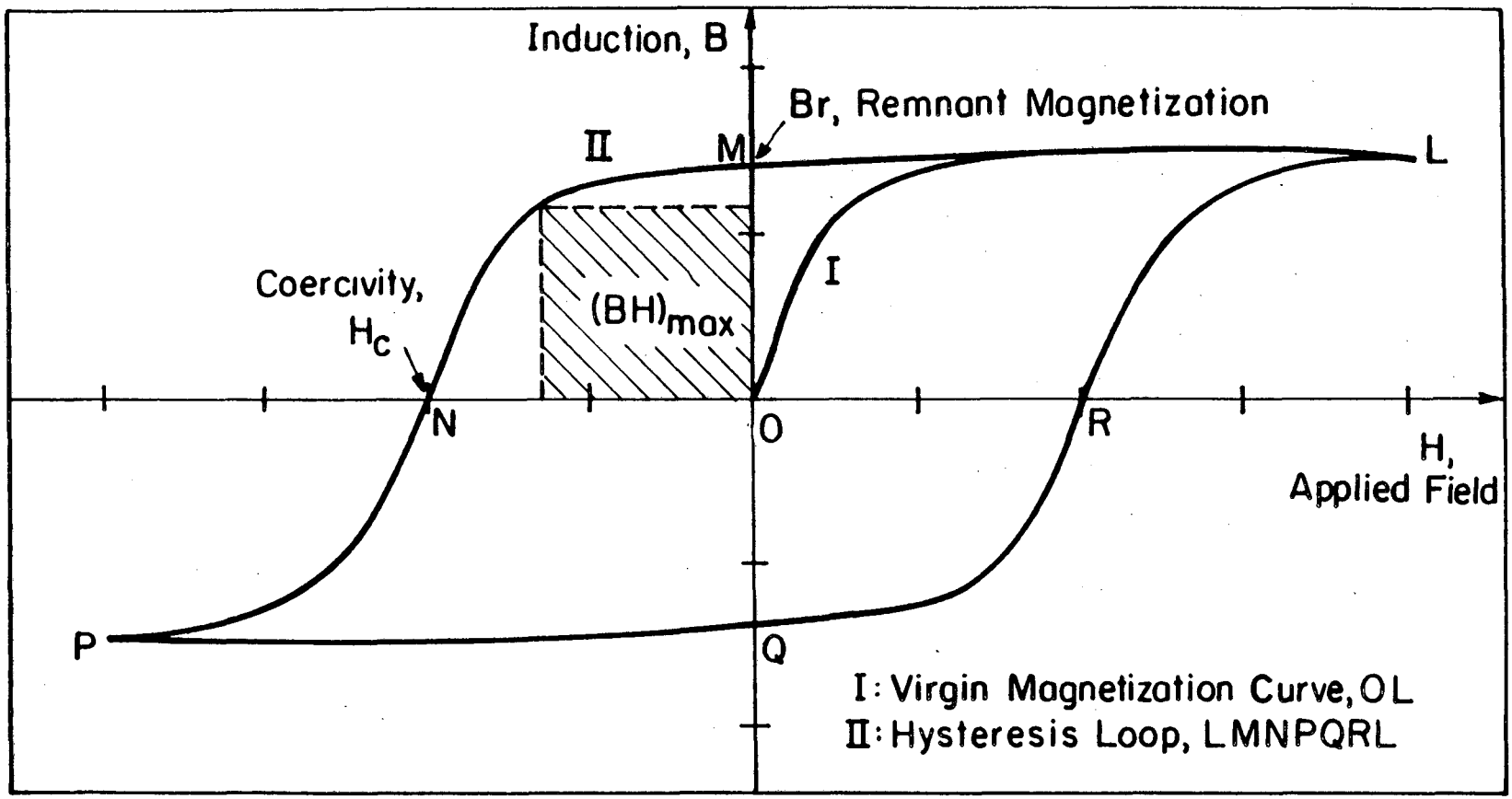

XBL8512-6870

Figure 1

APPLICATIONS OF PERMANENT MAGNETS

General property of magnets used	*More specific method of application*	*Particular devices*
Mechanical forces exerted by or on magnets	Torque on magnet in magnetic field	Compass. magnetometer
	Attraction between magnet and iron or other magnets	Holding devices, notice boards, games, door catches. Magnetic filtration, retrieval devices, drives and couplings, window cleaning, switches, thermostats, thickness gauges, magnetic tools
	Attraction induced between other iron parts	Reed switches, railway warning systems, magnetic clutches
	Repulsion: magnet and magnet	Bearings (some bearings now use attraction) levitated transport, toys
	Electromagnet and magnet	Brake for coil winder etc.
	Induced repulsion	Sheet floater
Electromagnetic forces	Moving coil devices	Loudspeakers and telephone receivers. Instruments. DC motors
	Moving magnet devices	Synchronous and brushless motors, clocks, hysteresis motors
	Moving iron devices	Some telephone receivers, polarized relays
Electromagnetic induction	Relative motion coil and magnet	Flux measurement. Generators, sensing devices. Microphones, pick-ups
	Eddy currents	Damping devices, brakes, speedometers
Forces on moving electrons and ions	Focusing	TV (now little used) electron microscope, klystron, travelling-wave tube
	Crossed field action	Blow-out on switches, magneto-hydrodynamics generator (see generators). Magnetron, mass spectrometer, ion pump, omegatron, TV picture shift
Magneto-optical effects	Kerr and Faraday effects	Domain studies, Memory stores, Other possible devices
Magnetic resonance	NMR	Chemical analysis. Accurate field measurements. Magneto-crystalline anisotropy
Action of magnetic fields on solid and liquid media	Magnets in magnetic circuits	Saturistors. Magnetizers and magnetic heat treatment
	Electronic and semi-conductor	Wave guides, circulators. Hall and magnetoresistance devices
Biological and chemical effects		Research on influence of magnetic fields on life processes. Water conditioners

Table 1 (1)

APPLICATIONS

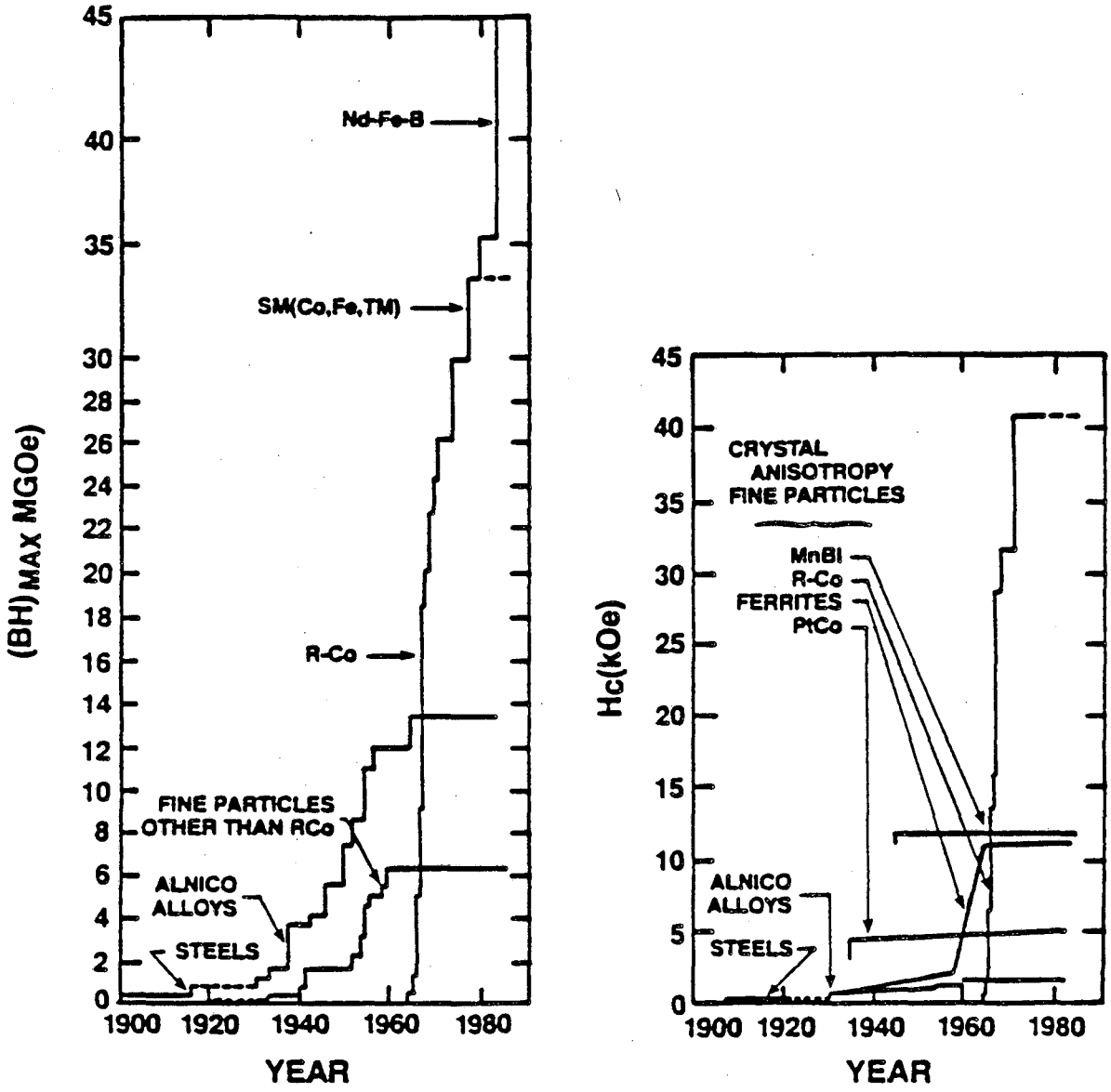

XBL 879-3978

Figure 2

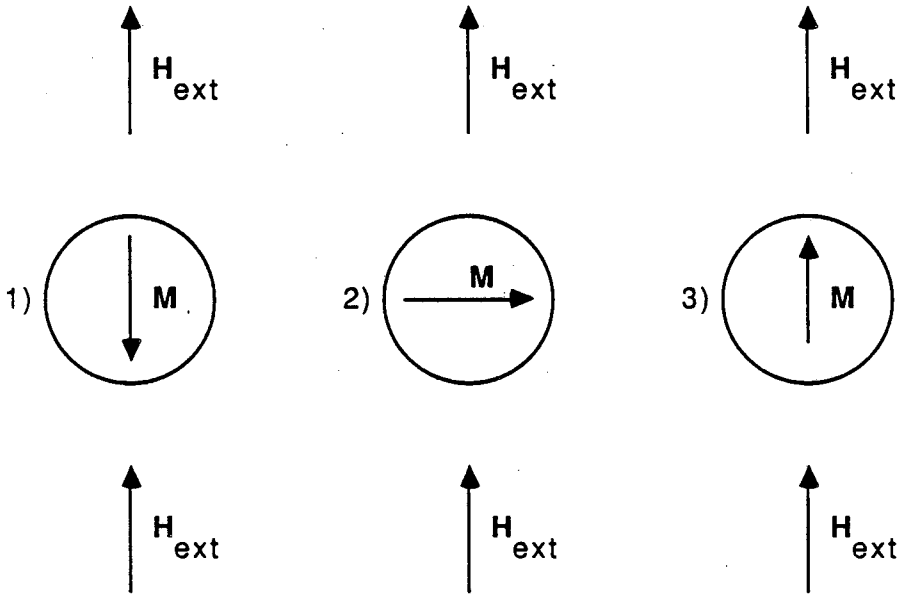

Uniform Rotation

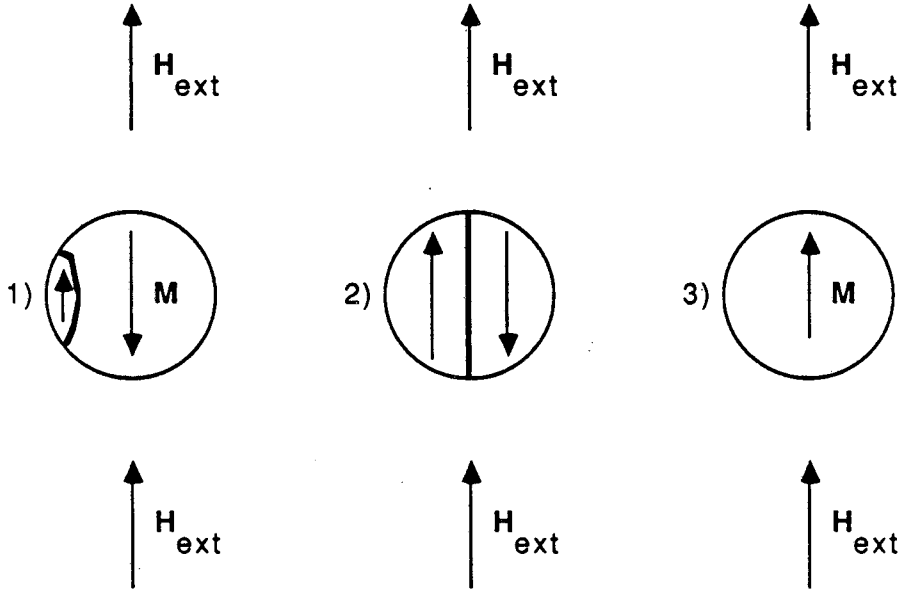

Domain Wall Nucleation and Growth

XBL 879-3892

Figure 3

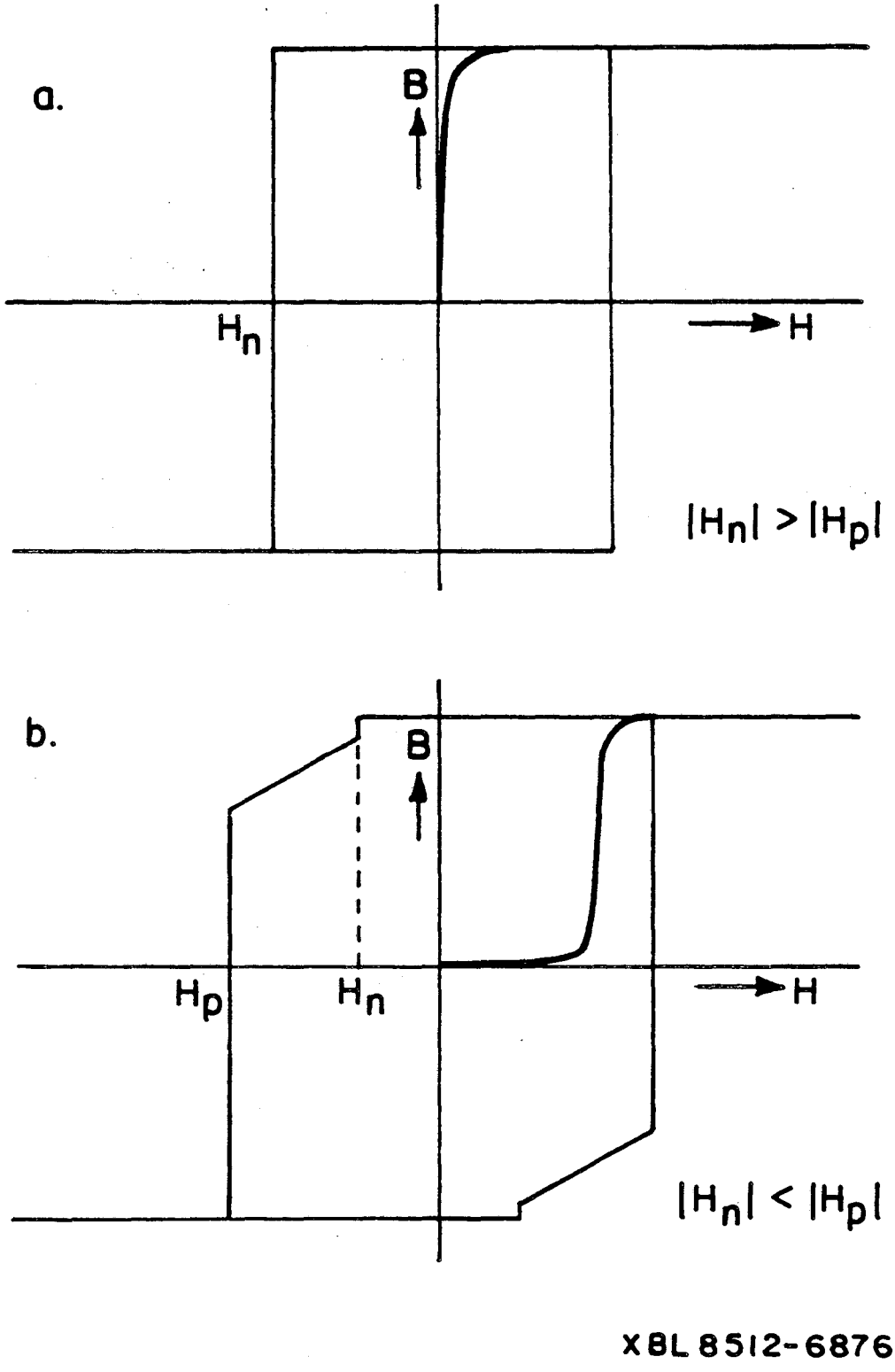

Figure 4

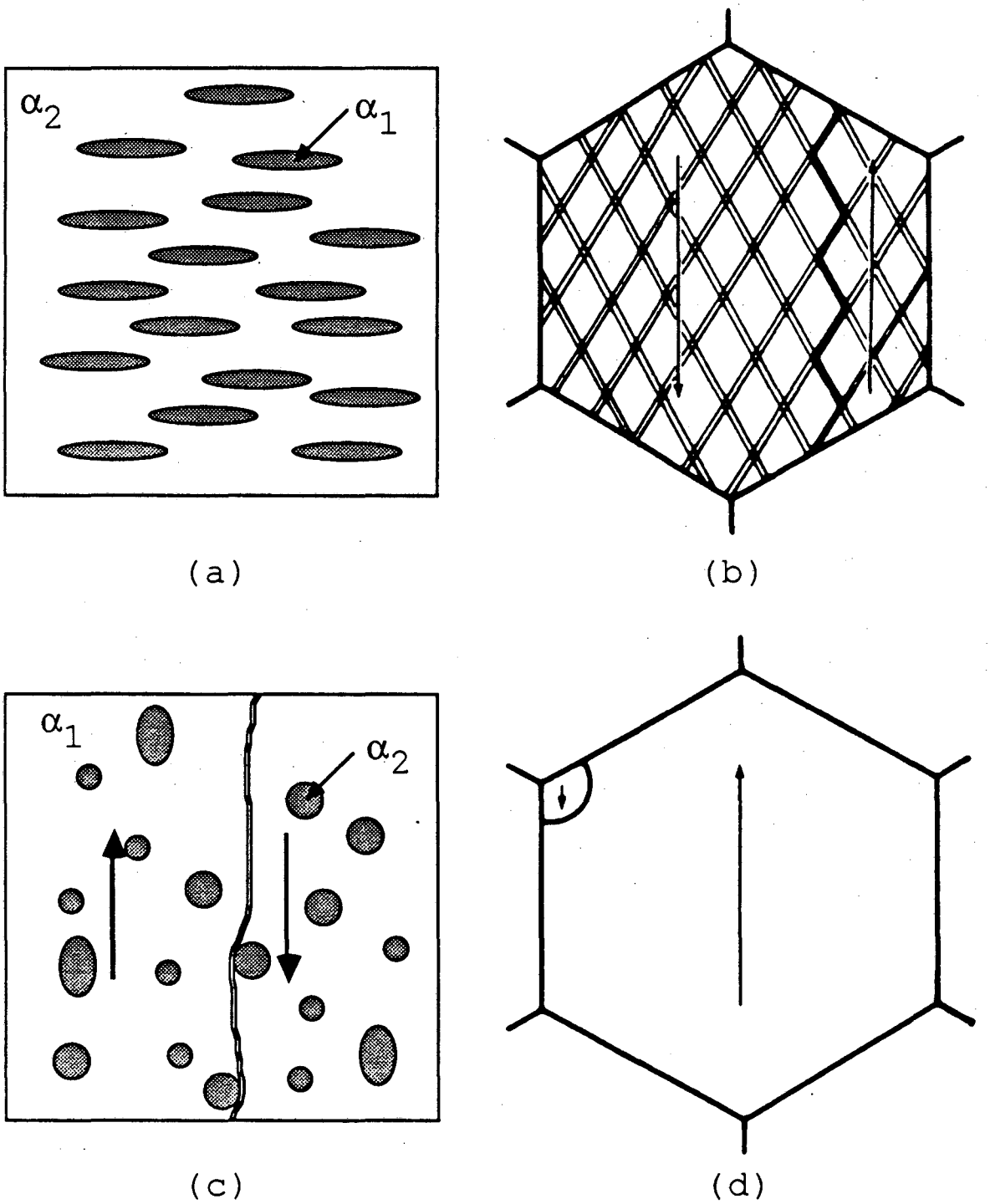

XBL 8710-4020

Figure 5

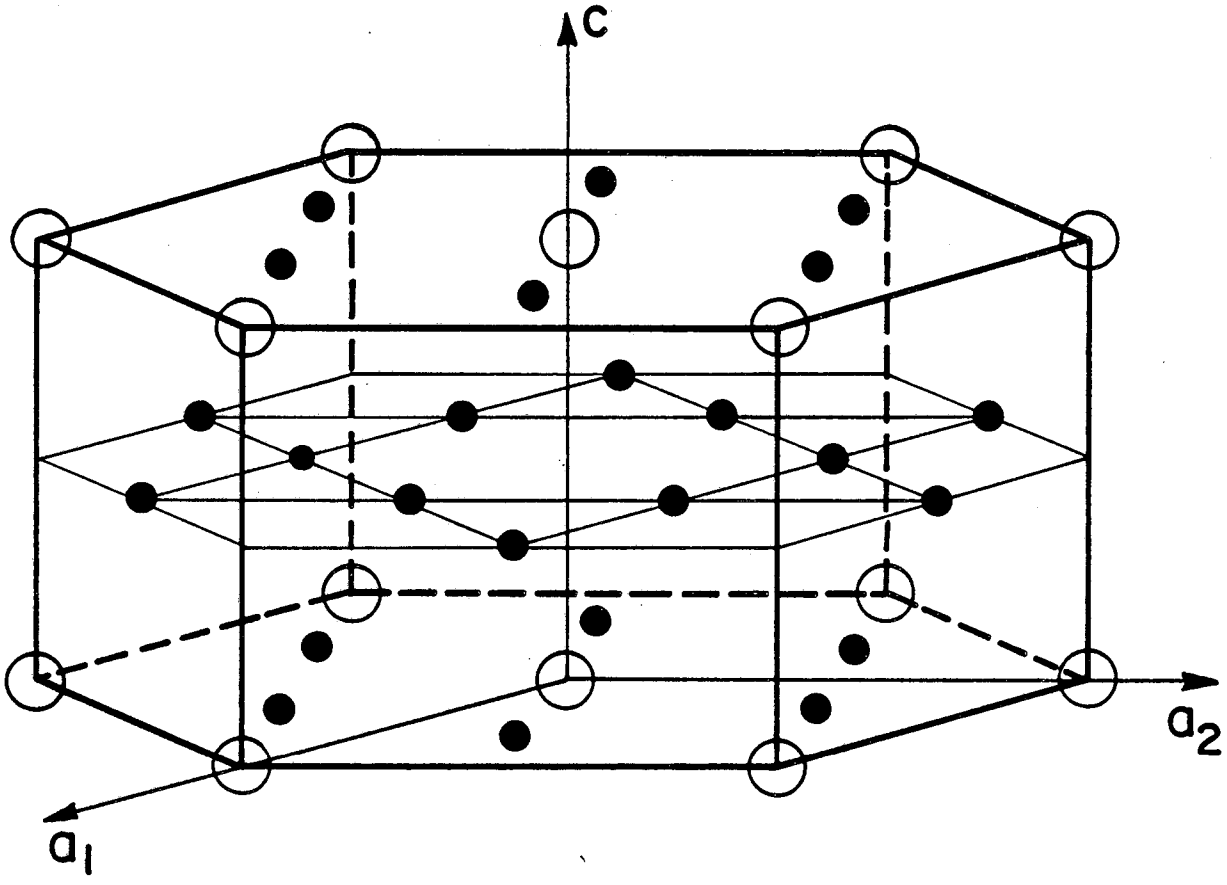

$SmCo_5$ Conventional Unit Cell
(Perspective Drawing)

○ Sm
● Co

XBL 831-5004

Figure 6a

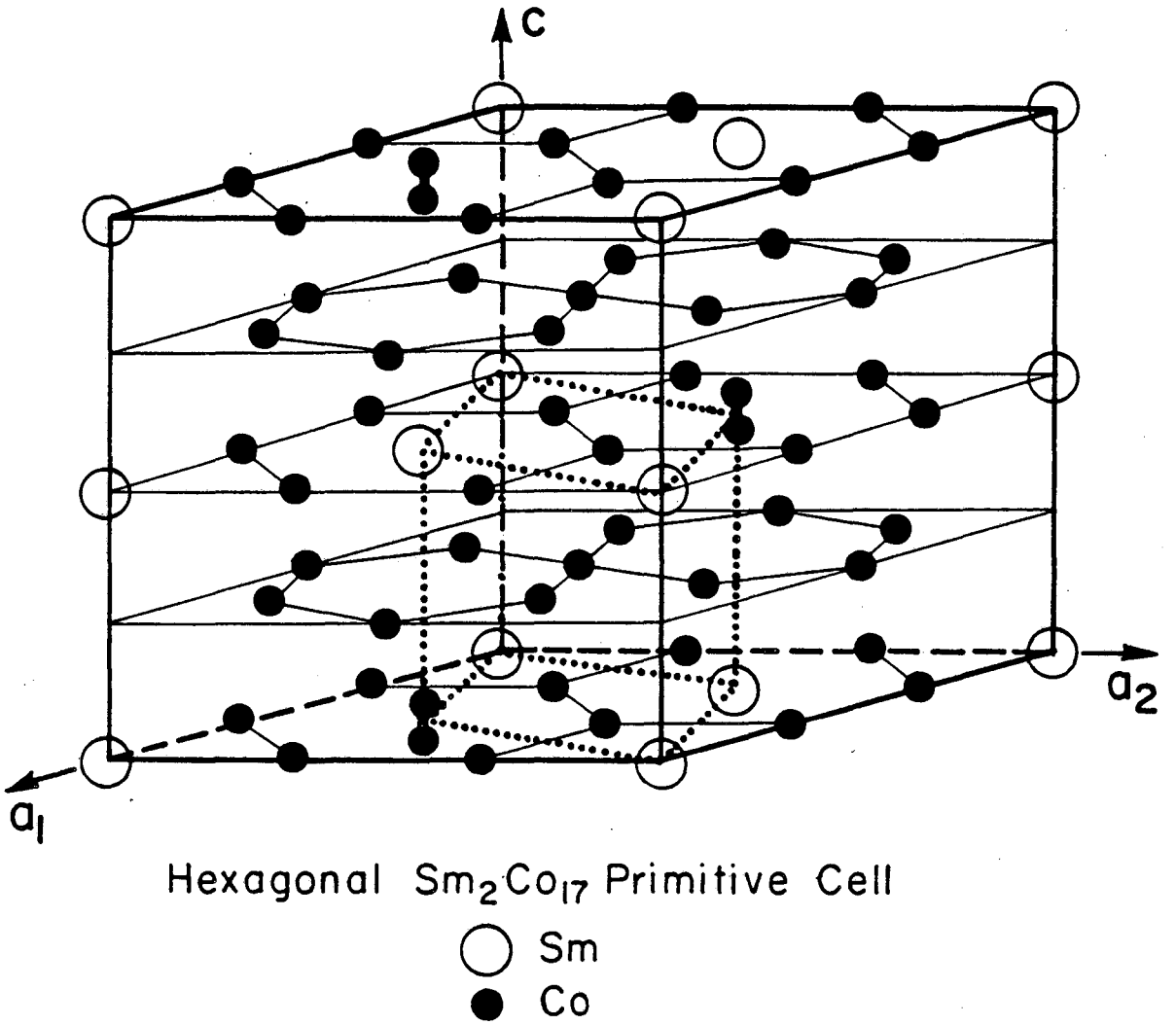

Figure 6b

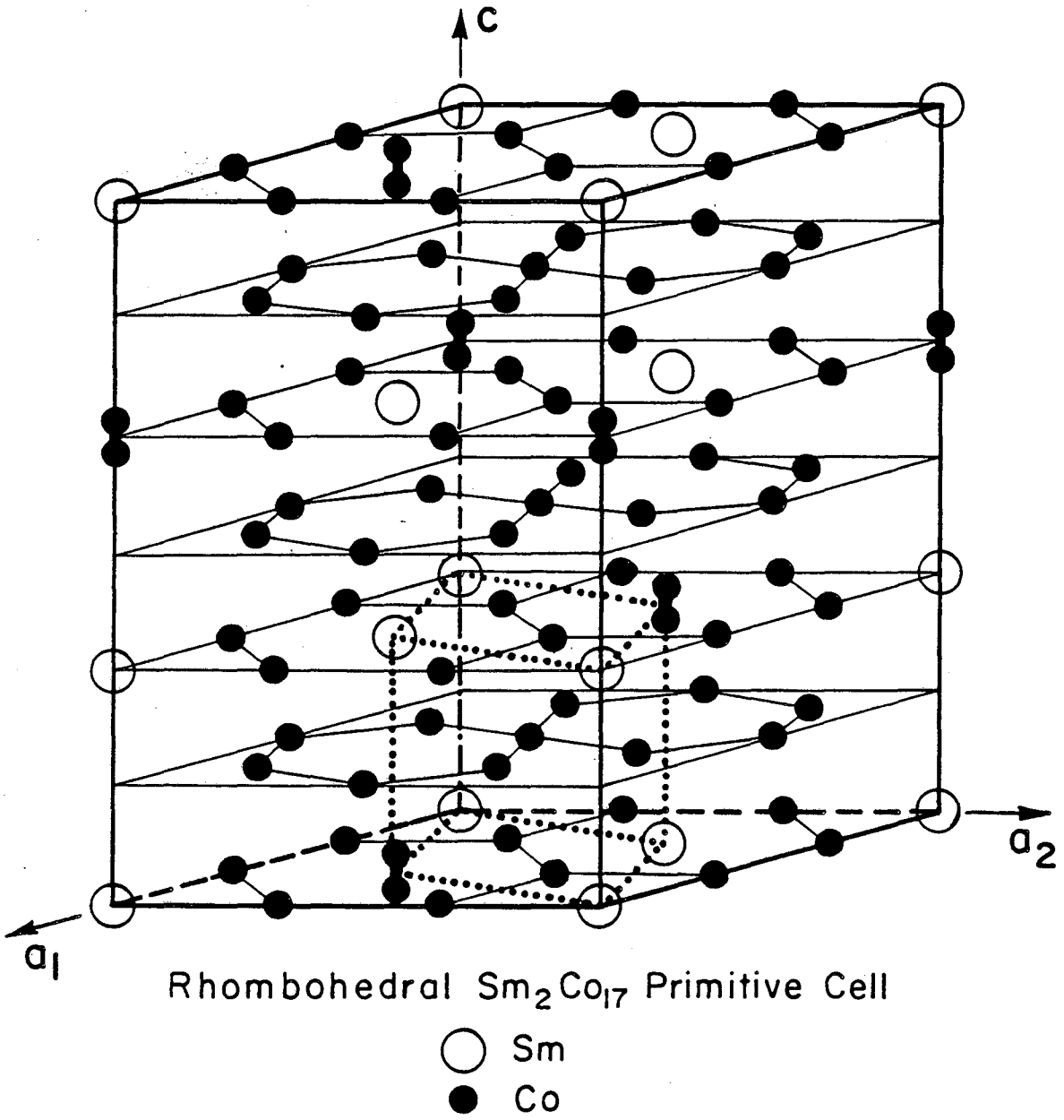
c
a2
a1
Rhombohedral Sm2Co17 Primitive Cell
Sm
Co
XBL 831-5007

Figure 6c

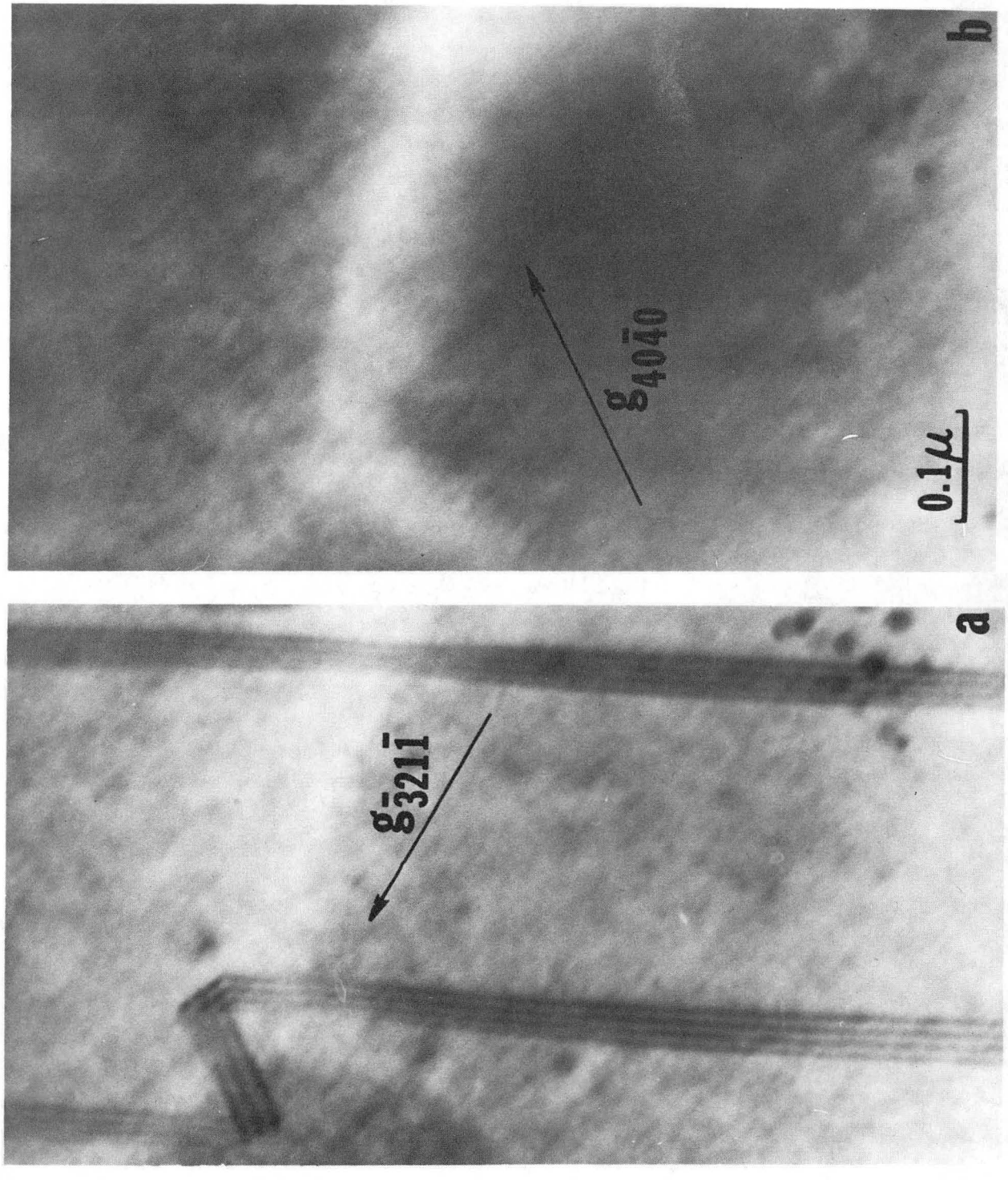

XBB 770-9735

Figure 7

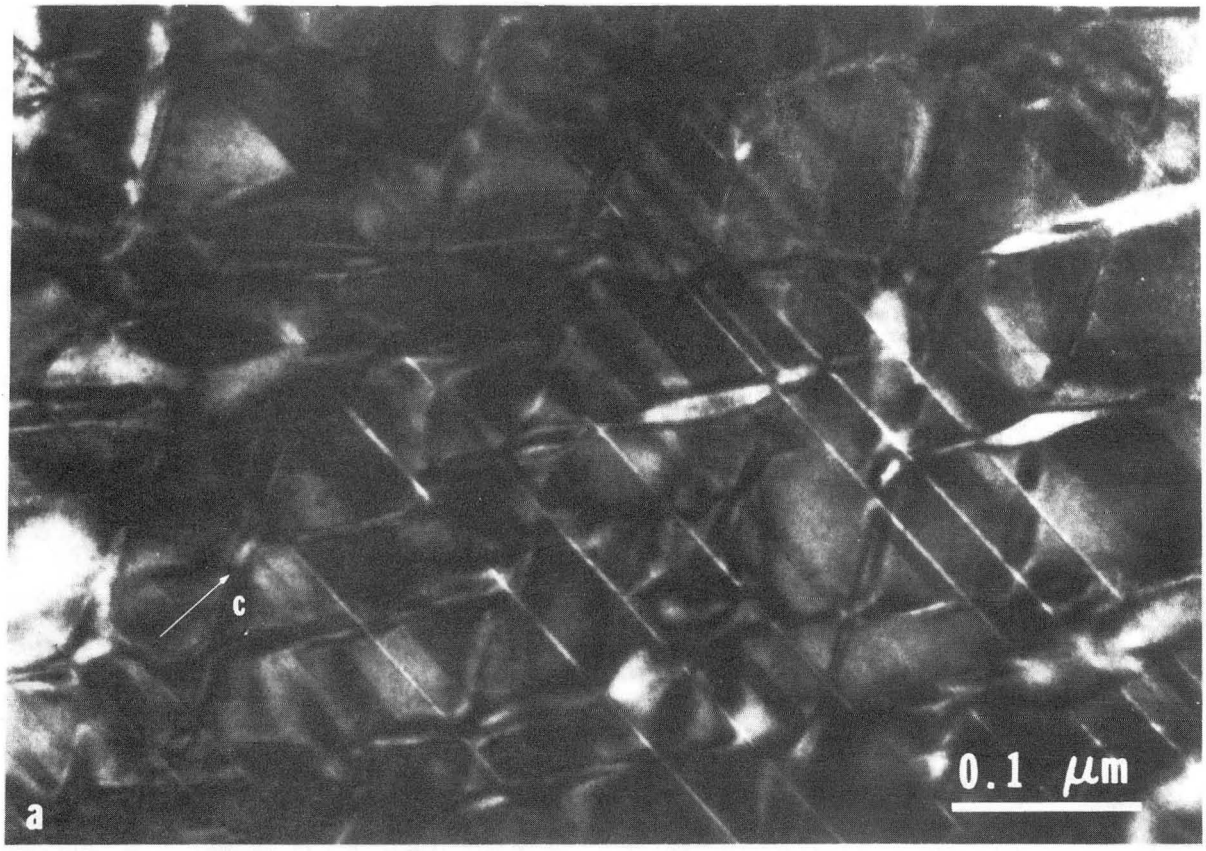

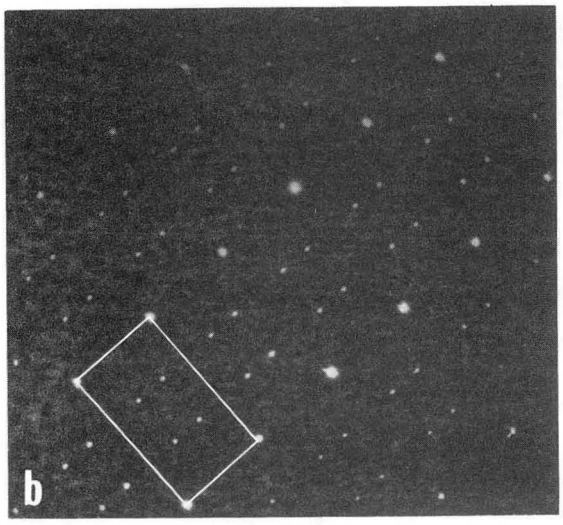

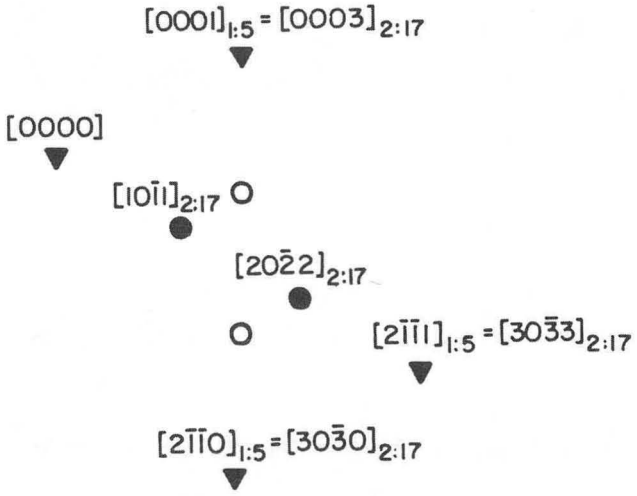

Figure 8

XBB 810-9499

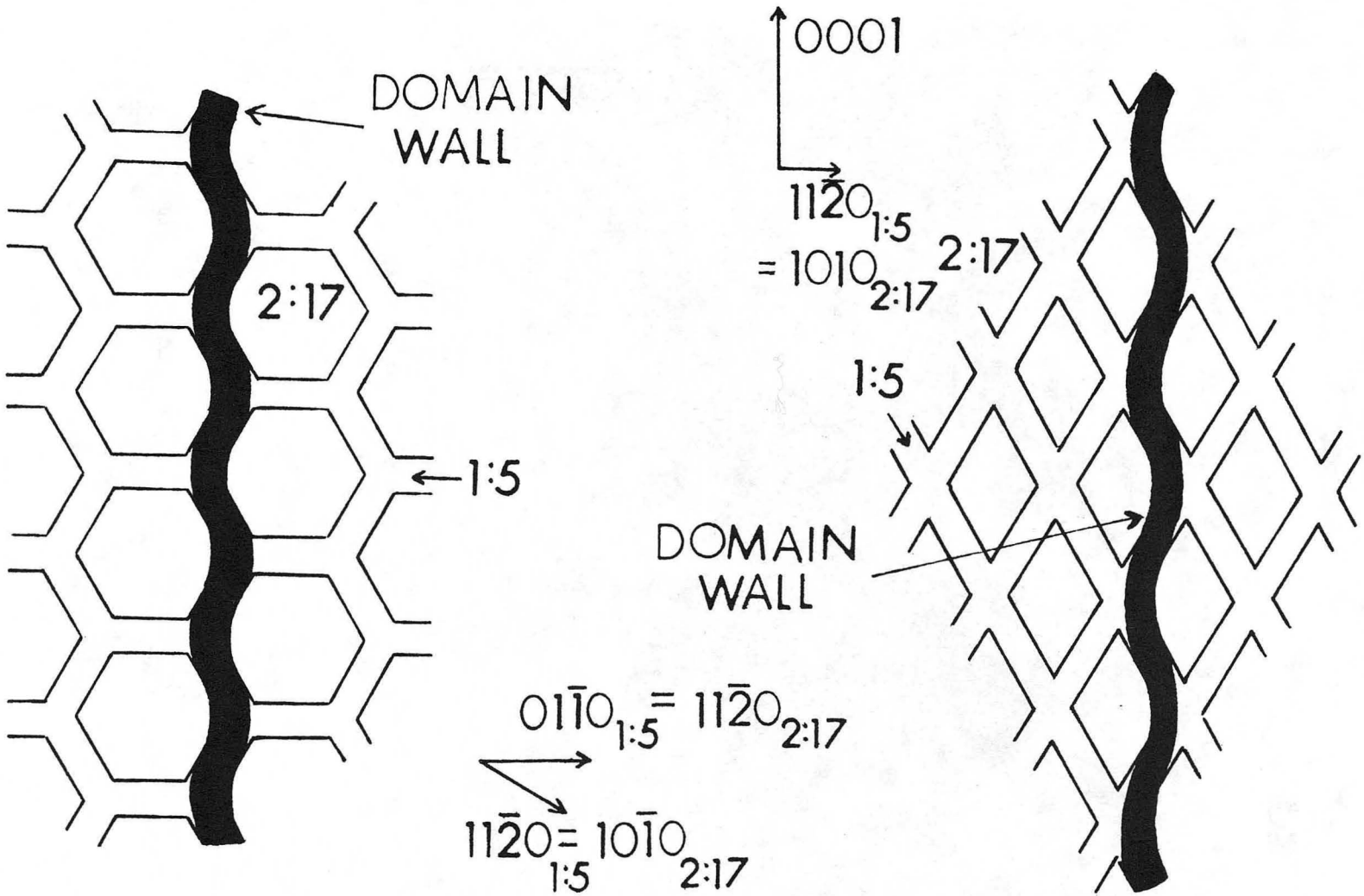

XBL 836-10121

Figure 9

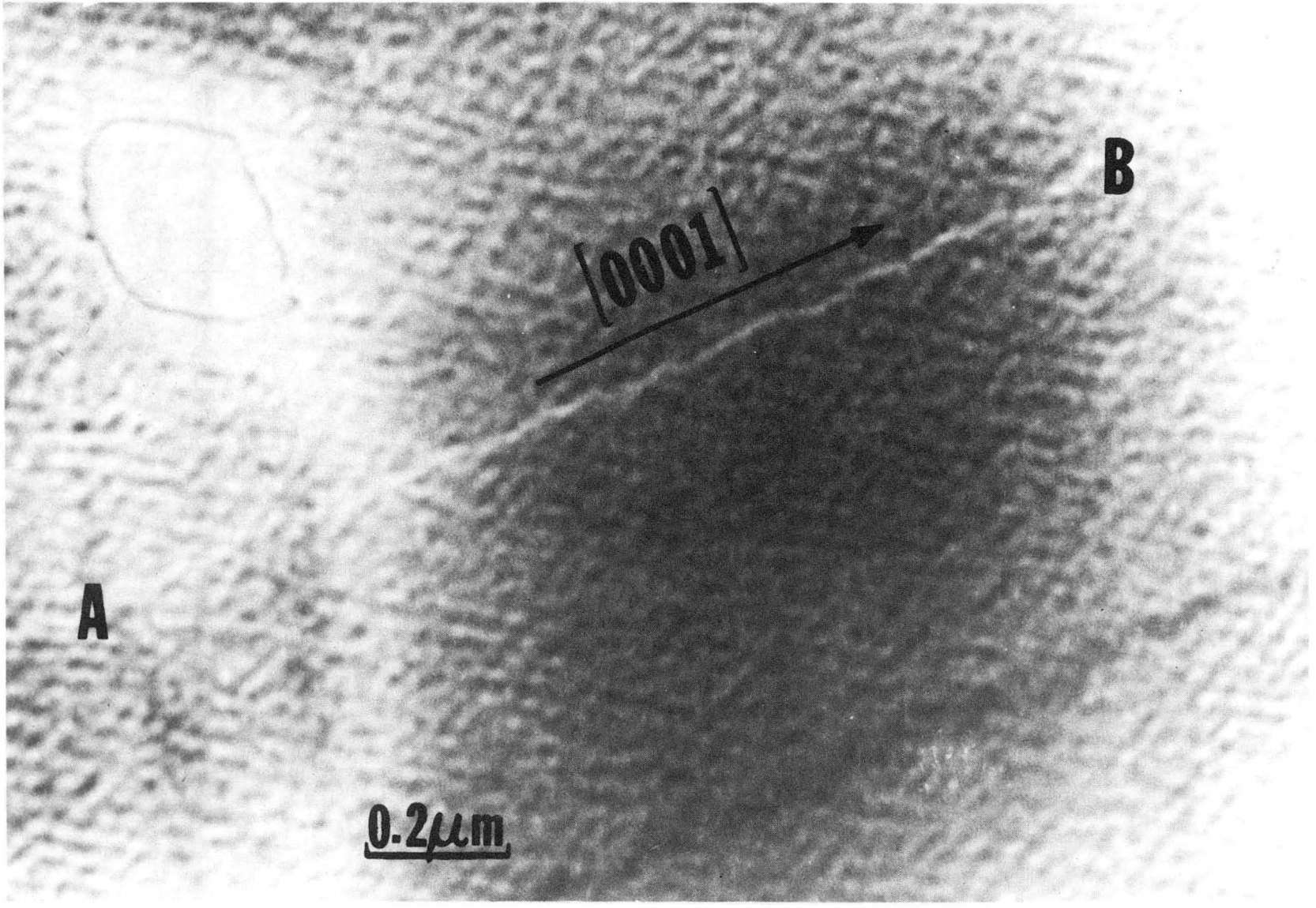

Figure 10

XBB 795-6614

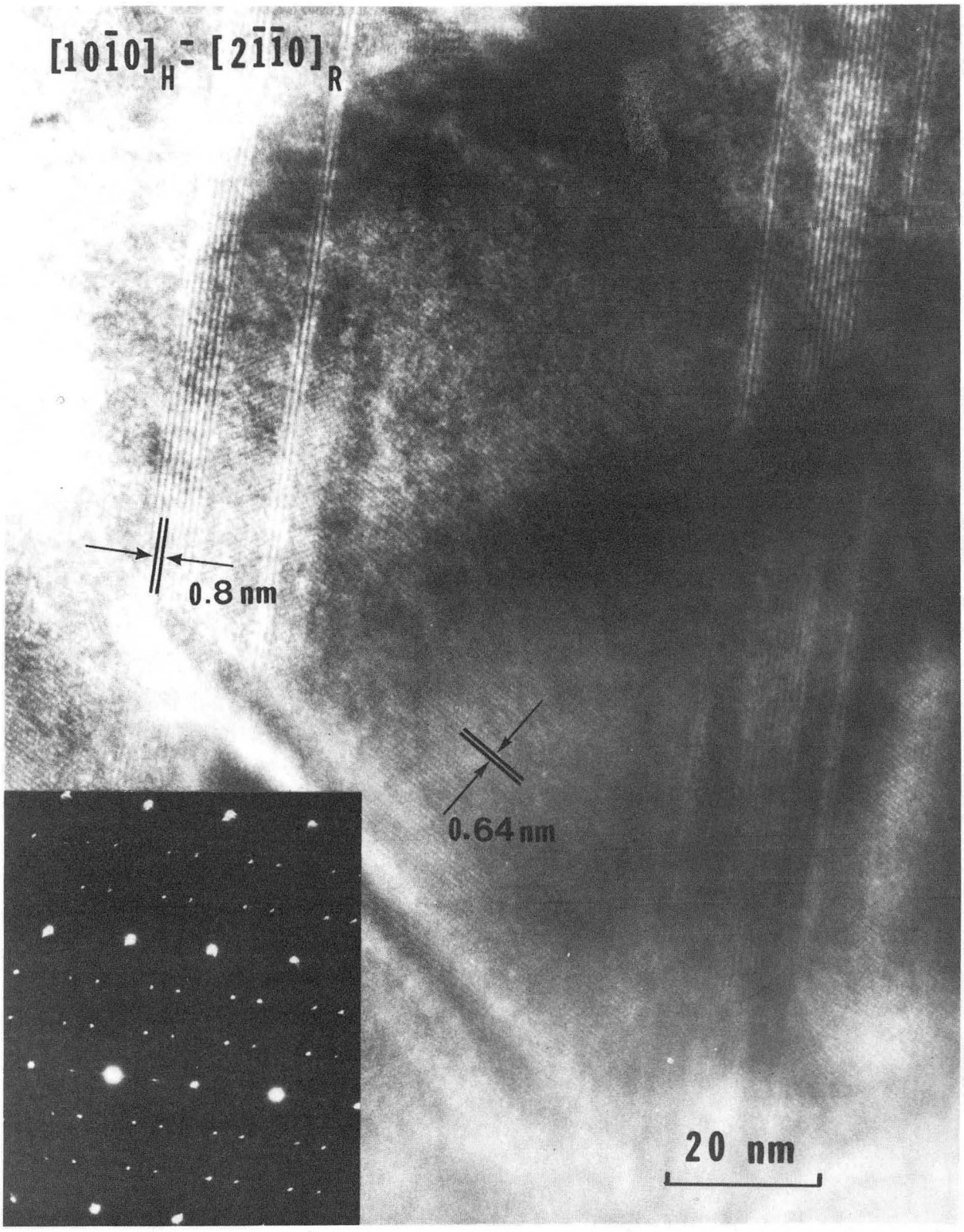

Figure 11 XBB 810-10172

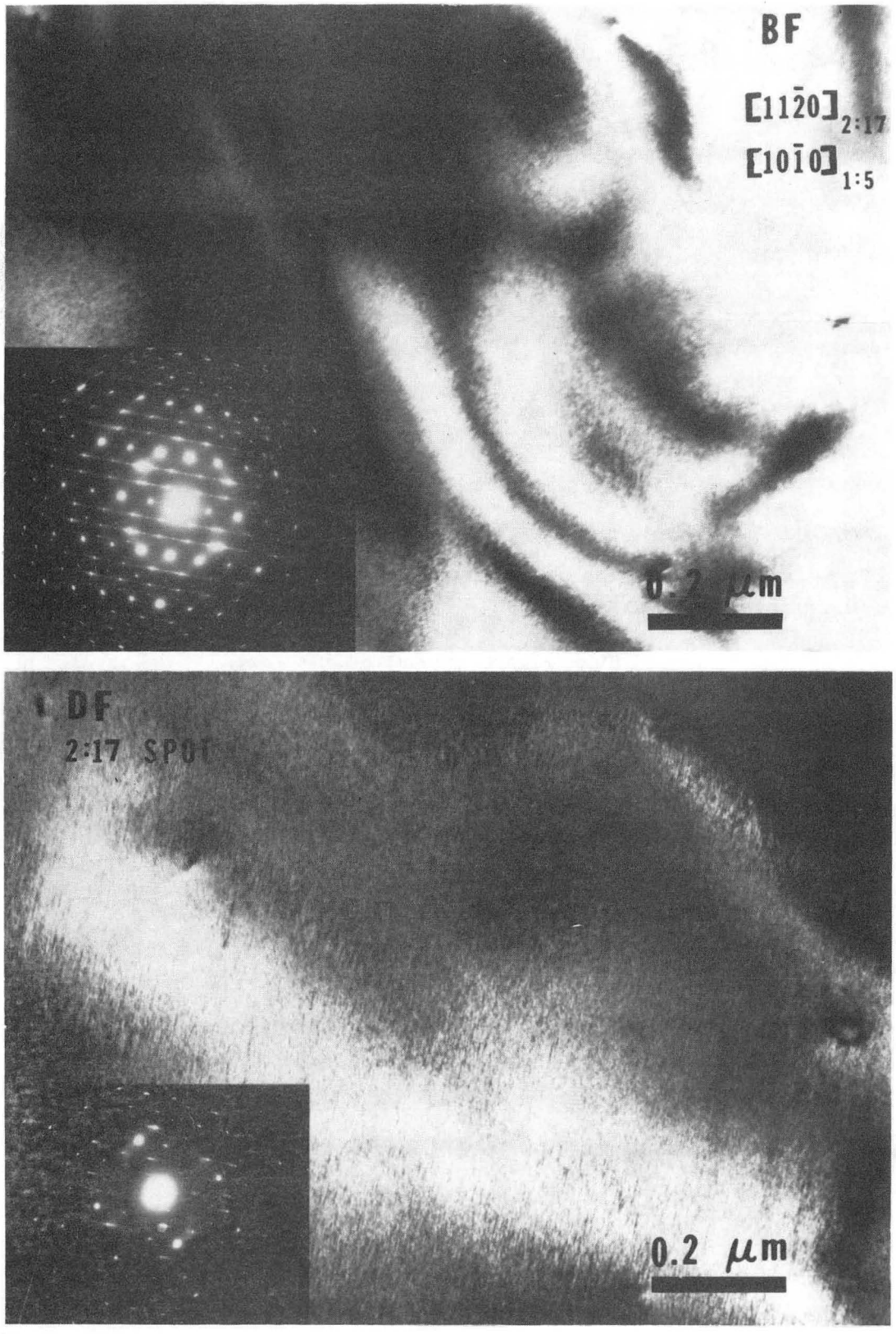

Figure 12 XBB 820-10201

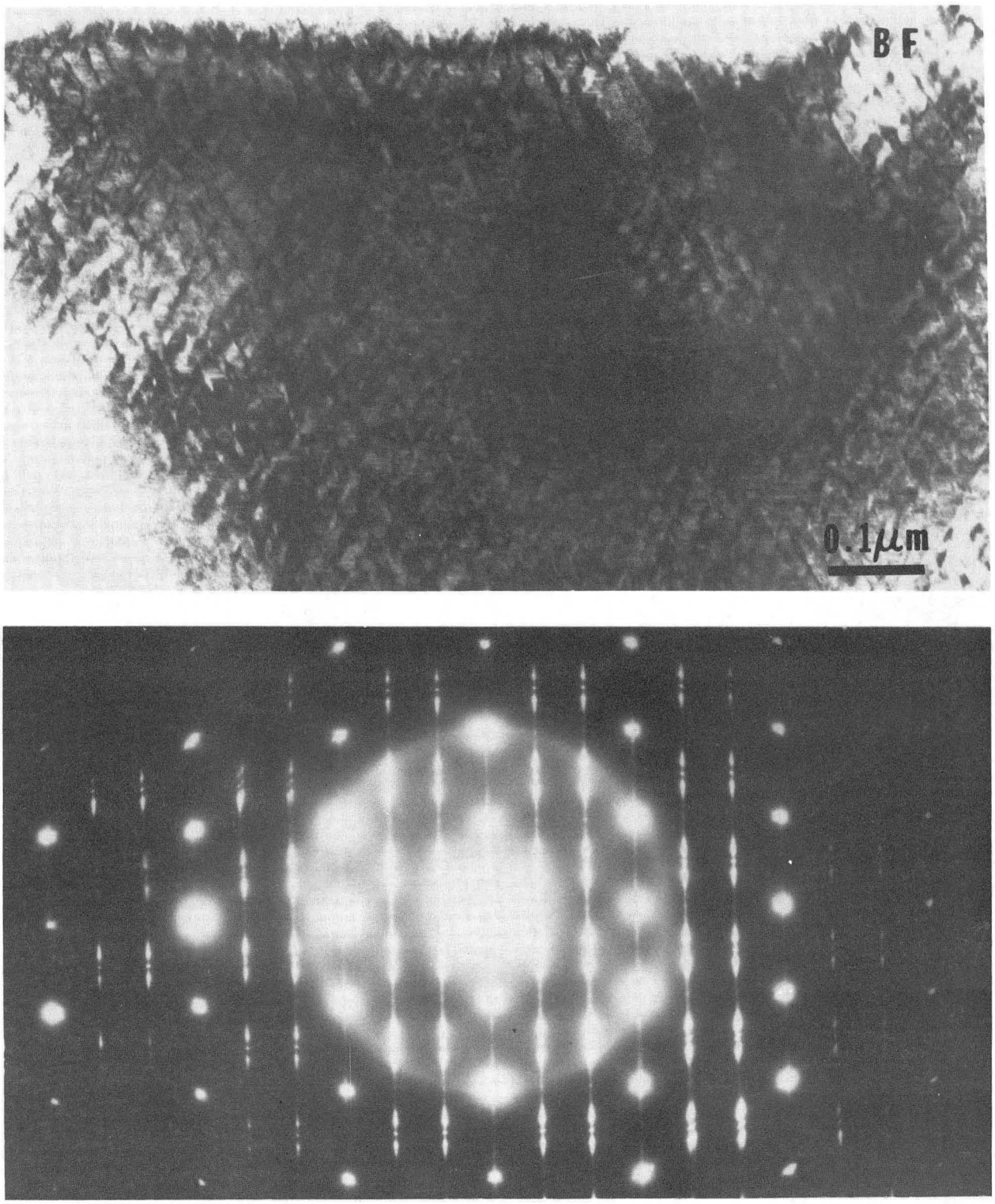

Figure 13 XBB 820-10198

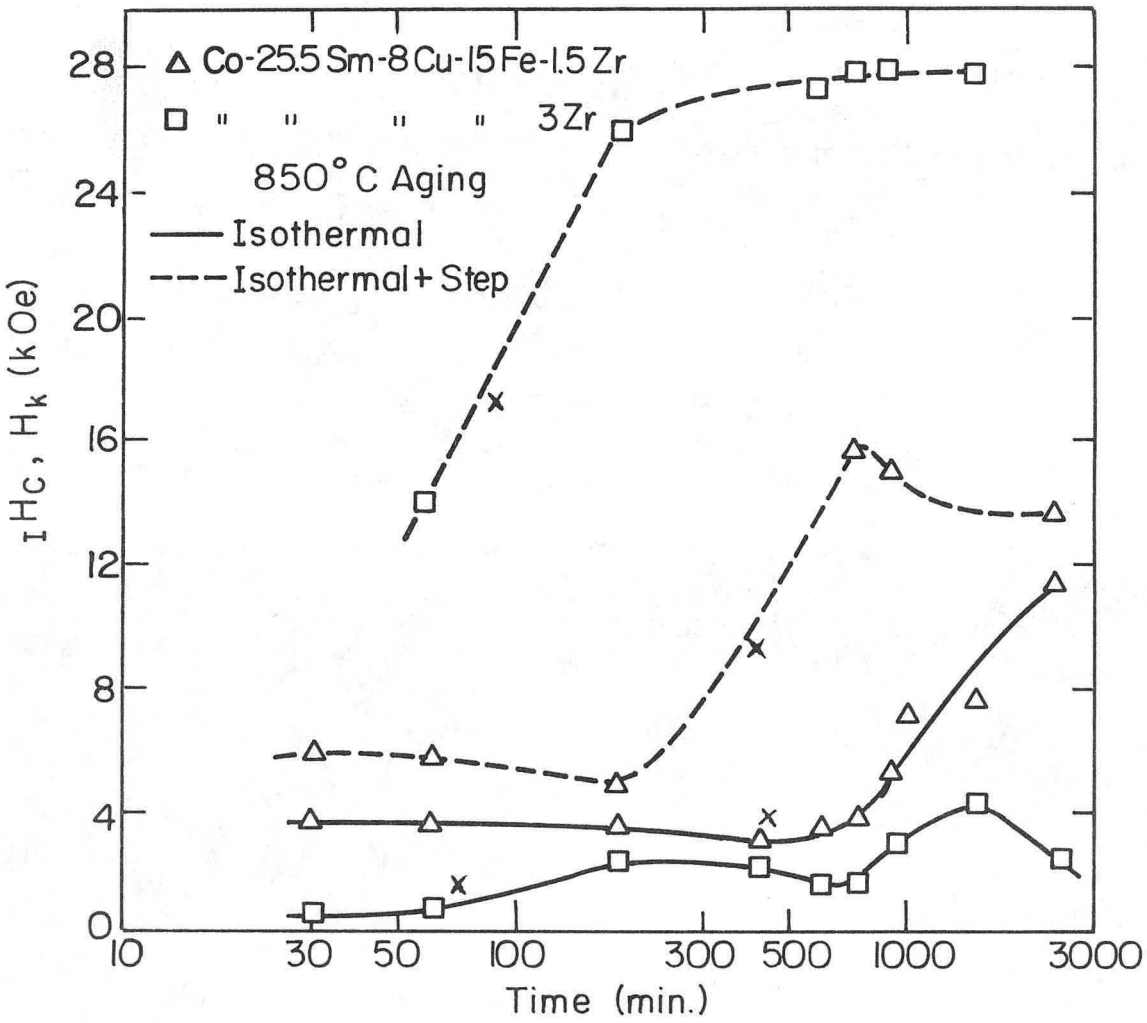

XBL 809-5787

Figure 14

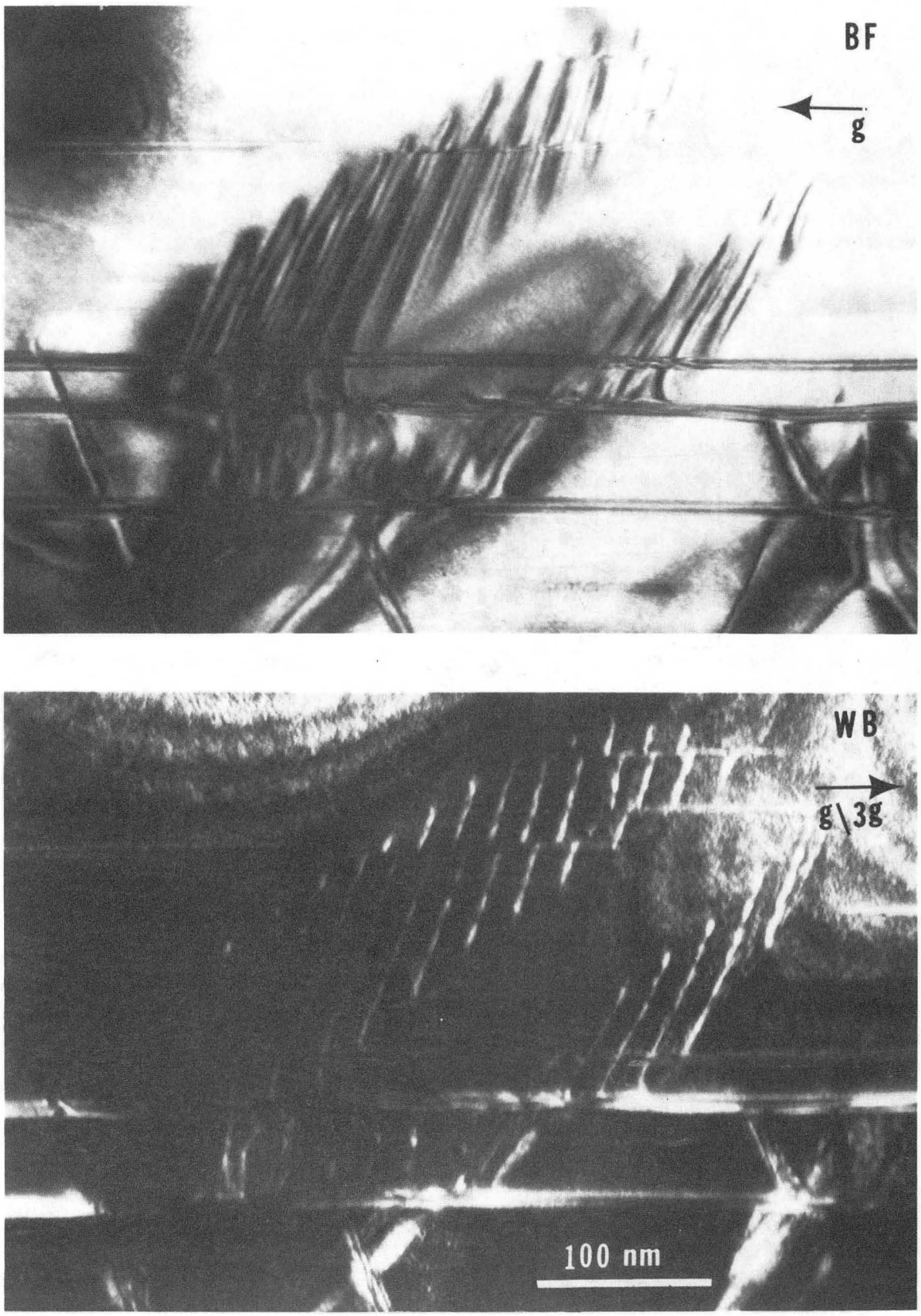

Figure 15 XBB 835-4362

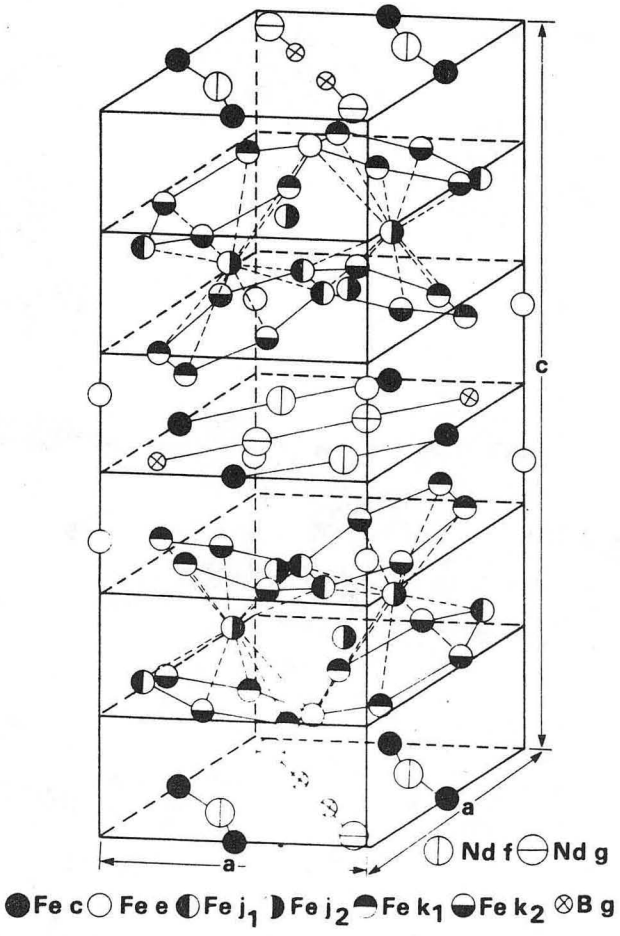

Figure 16a

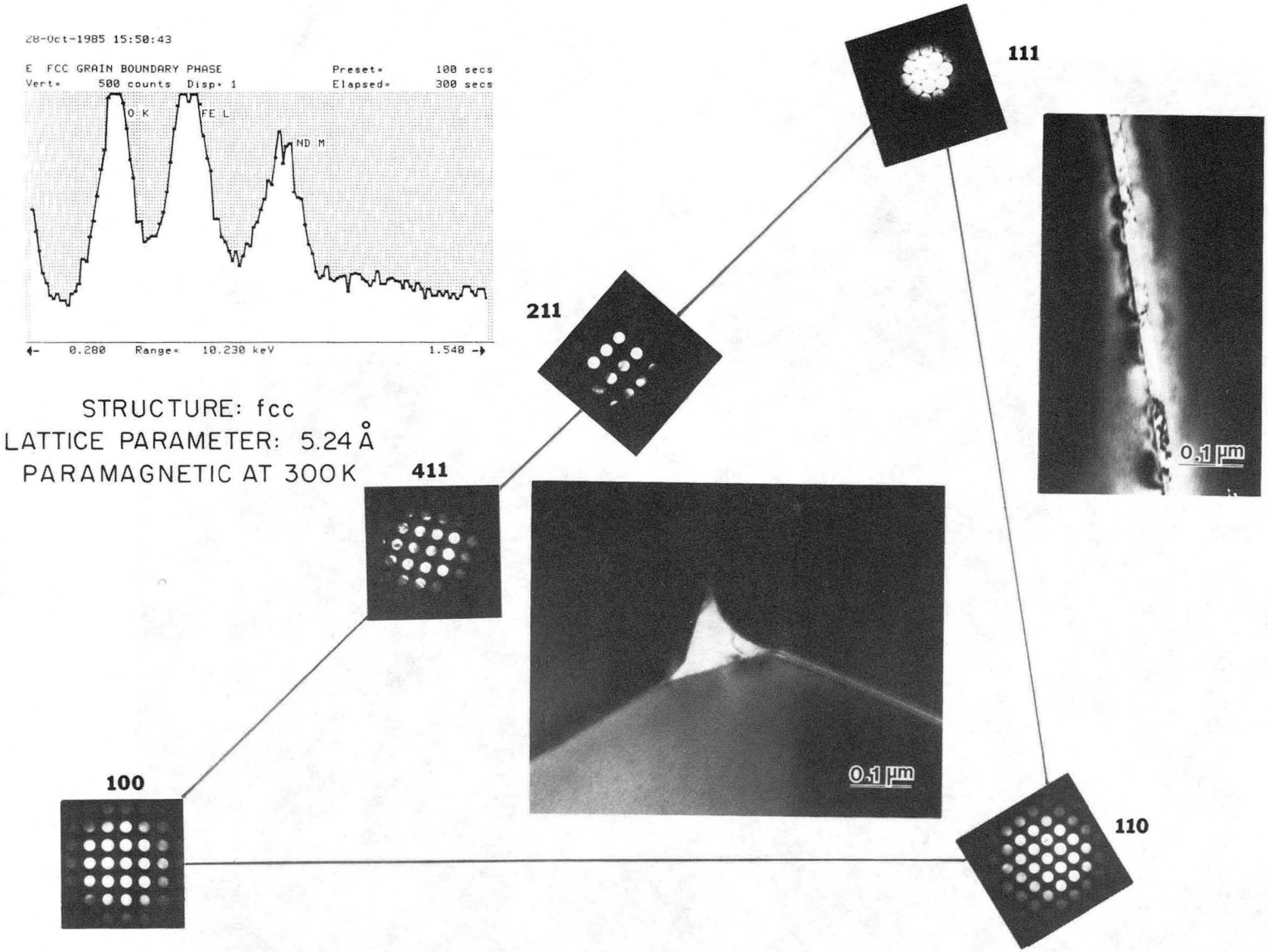

Figure 16b

XBB 856-4526B

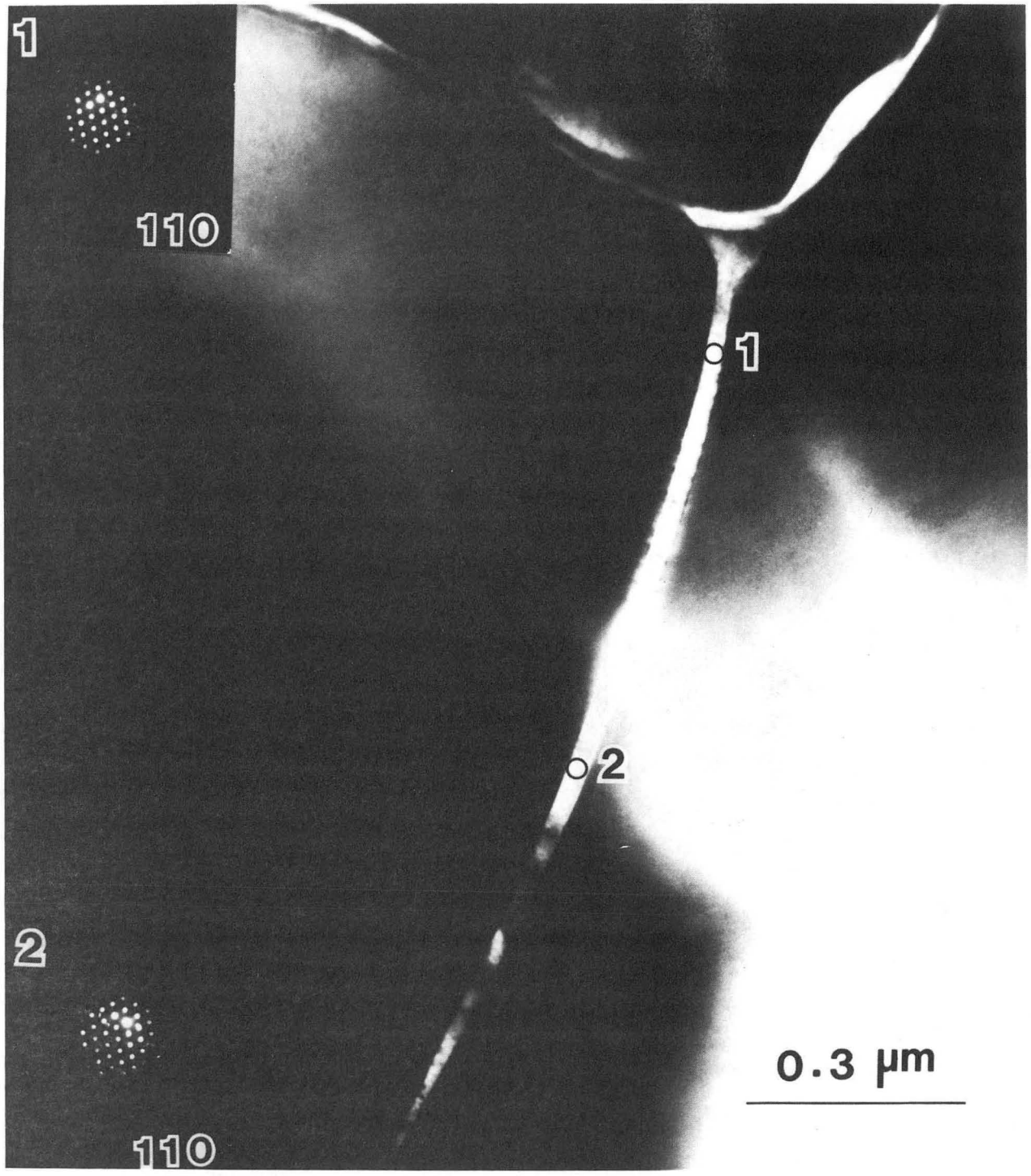

Figure 17

XBB 865-3635

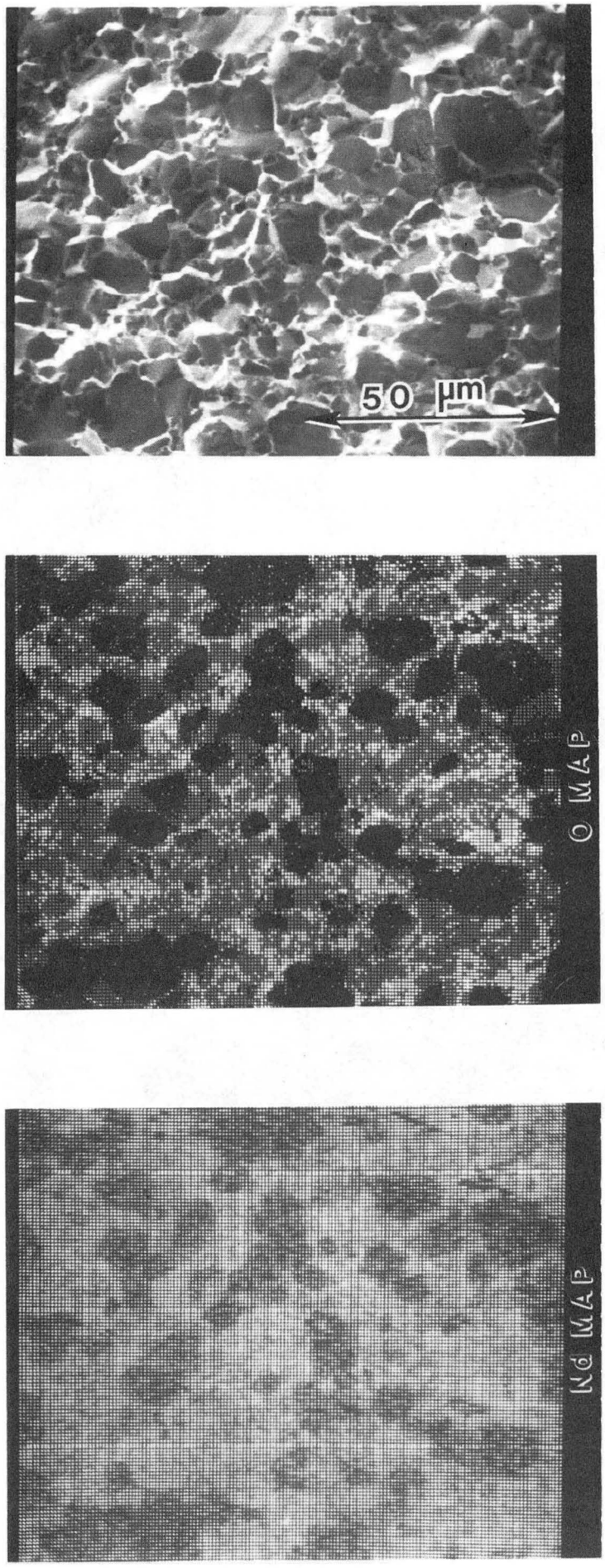

Figure 18

XBB 850-10300

Figure 19

XBB 874-2622

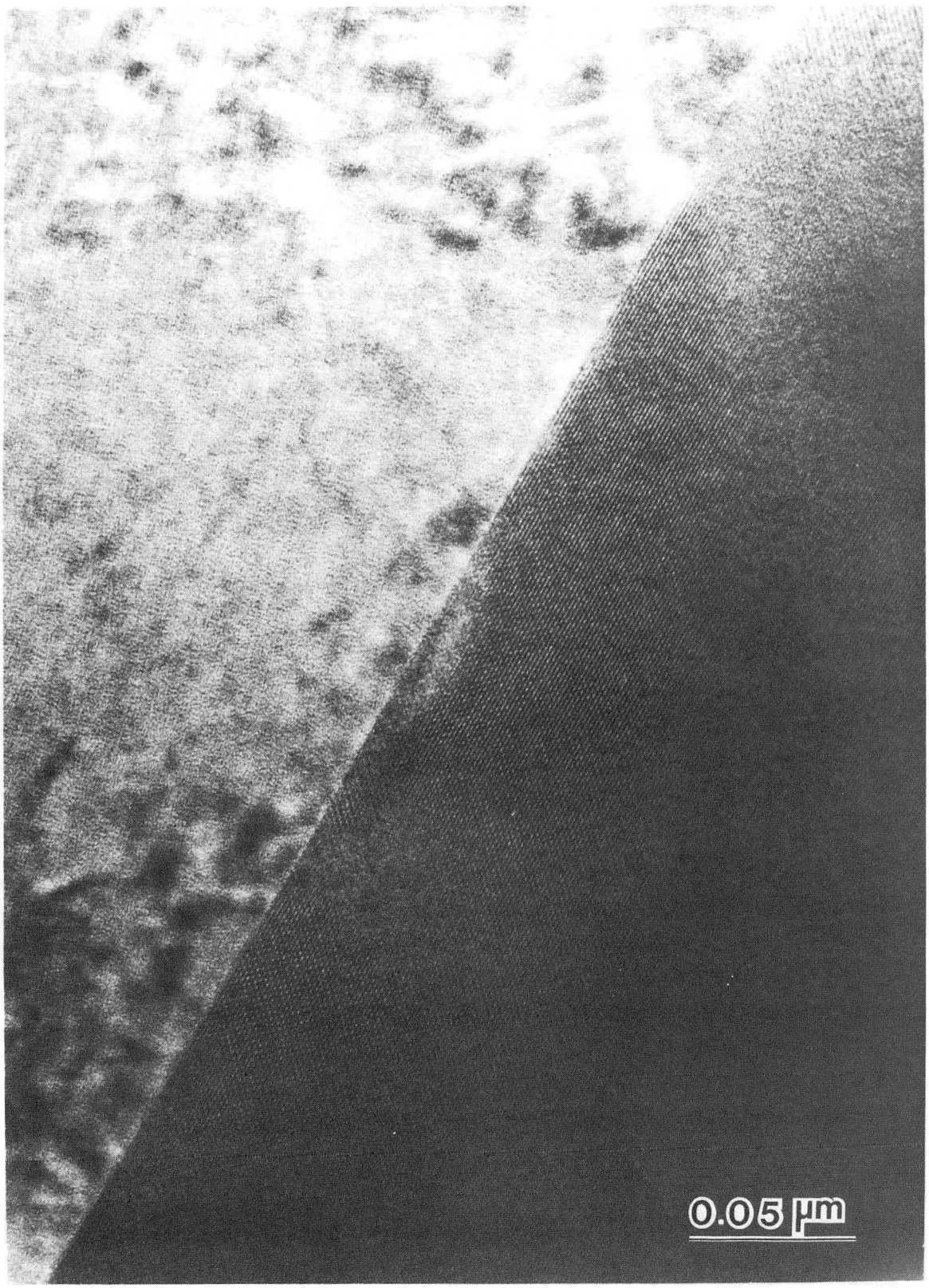

Figure 20a

XBB 862-1140

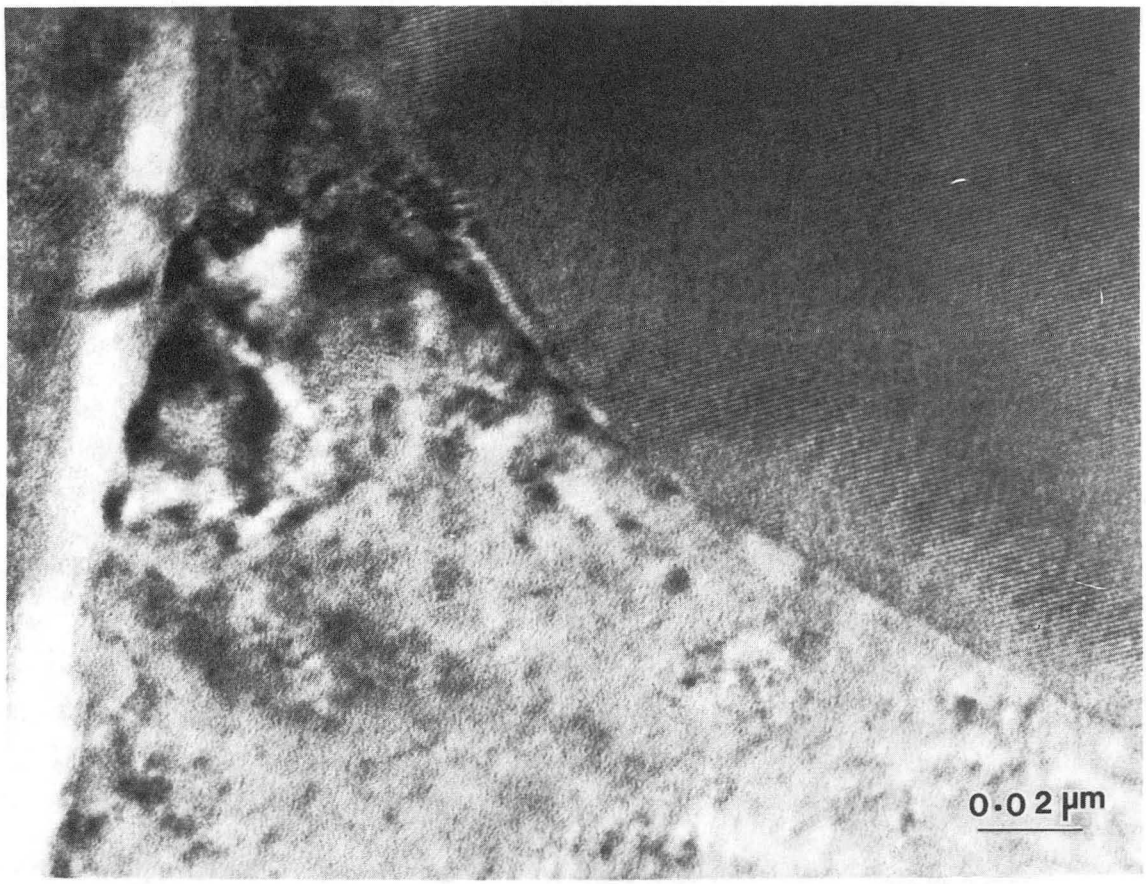

XBB 862-1435

Figure 20b

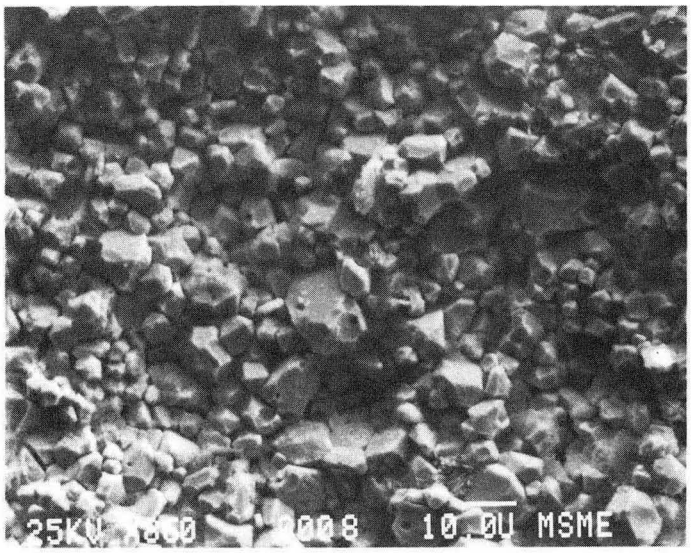

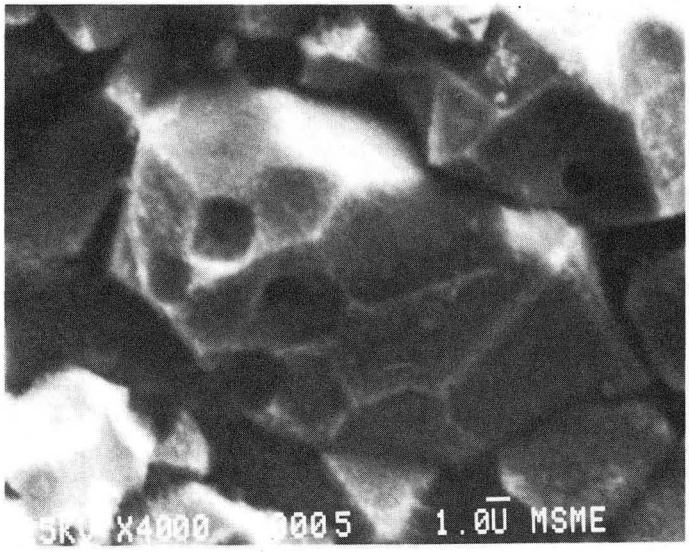

XBB 876-4484

Figure 21

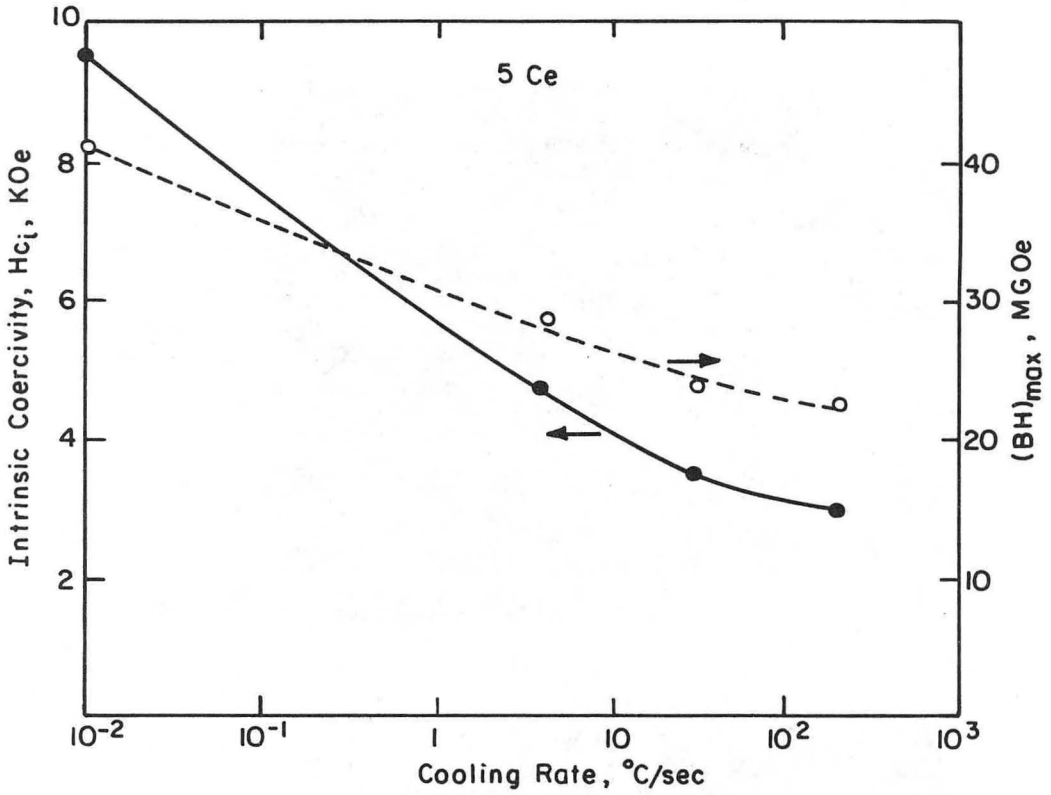

XBL 8510-6759 A

Figure 22

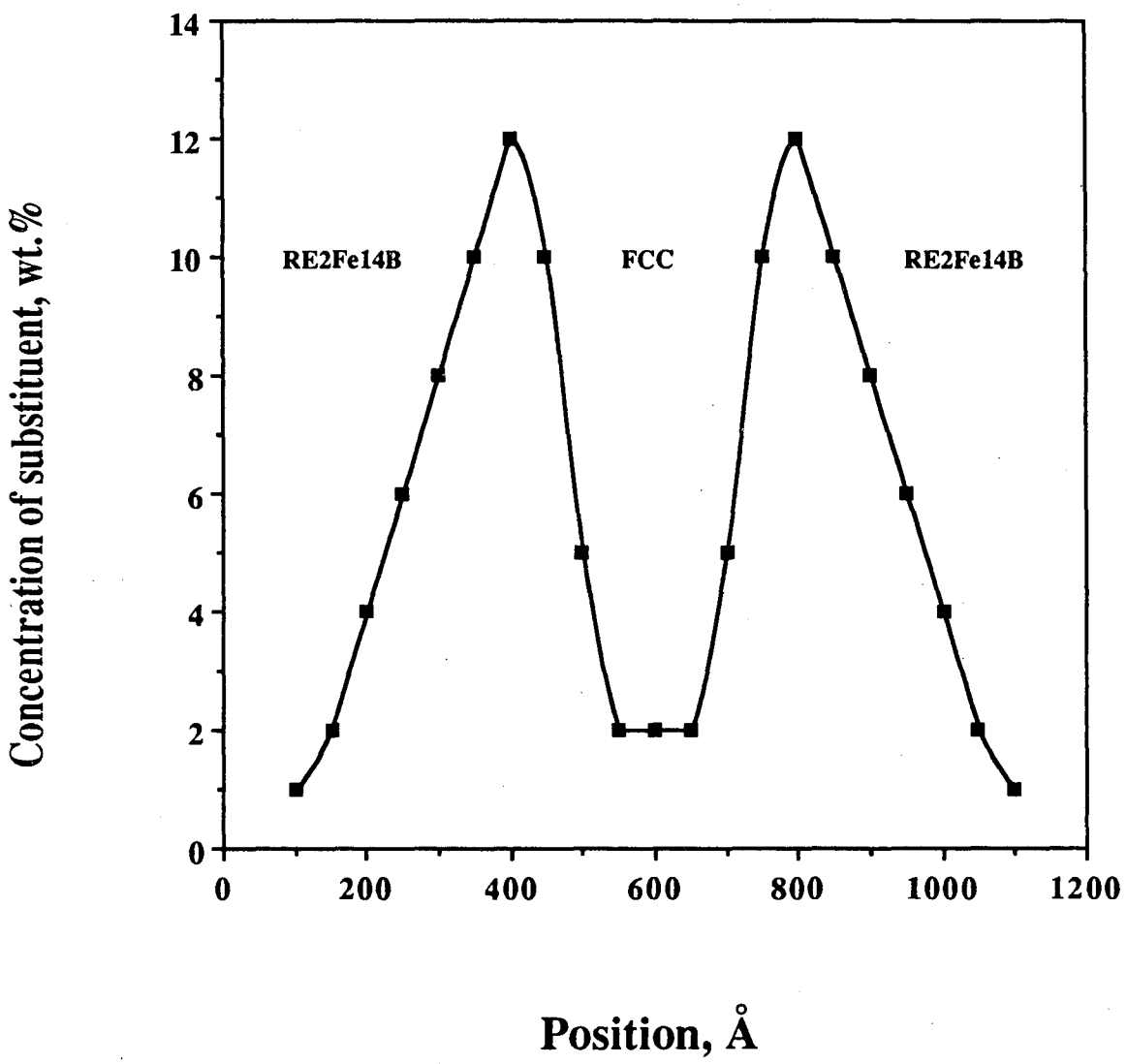
14
12
10
8
6
4
2
0
0
200
400
600
800
1000
1200
RE2Fe14B
FCC
RE2Fe14B
Concentration of substituent, wt.%
Position, Å

Figure 23

LAWRENCE BERKELEY LABORATORY
TECHNICAL INFORMATION DEPARTMENT
UNIVERSITY OF CALIFORNIA
BERKELEY, CALIFORNIA 94720